UC Santa Cruz

UC Santa Cruz Previously Published Works

Title

Subseafloor Temperature Variability During Ridge-Flank Hydrothermal Circulation: Implications for a Moderate-Temperature Earth System and Other Ocean Worlds

Permalink

https://escholarship.org/uc/item/7xw5n85j

Journal

Geochemistry Geophysics Geosystems, 27(10)

ISSN

1525-2027

Authors

Blackman, Donna K

Robinson, Kirt

Randolph-Flagg, Noah

et al.

Publication Date

2026-10-01

DOI

10.1029/2026gc012972

Copyright Information

This work is made available under the terms of a Creative Commons Attribution-NonCommercial License, available at https://creativecommons.org/licenses/by-nc/4.0/

Peer reviewed

eScholarship.org Powered by the California Digital Library
University of California

Check for updates

Geochemistry, Geophysics, Geosystems®

AGU ADVANCING EARTH AND SPACE SCIENCES

RESEARCH ARTICLE
10.1029/2026GC012972

Subseafloor Temperature Variability During Ridge-Flank Hydrothermal Circulation: Implications for a Moderate-Temperature Earth System and Other Ocean Worlds

Donna K. Blackman[1], Kirt Robinson[2], Noah Randolph-Flagg[3], Andrew T. Fisher[1], Julie A. Huber[4], Christopher R. German[5], and Kristin L. Dickerson[1]

[1]Department Earth and Planetary Sciences, University of California Santa Cruz, Santa Cruz, CA, USA, [2]School of Earth and Space Exploration, Arizona State University, Tempe, AZ, USA, [3]Department Earth and Environmental Sciences, University of Kentucky, Lexington, KY, USA, [4]Marine Chemistry and Geochemistry Department, Woods Hole Oceanographic Institution, Woods Hole, MA, USA, [5]Marine Geology and Geophysics Department, Woods Hole Oceanographic Institution, Woods Hole, MA, USA

Abstract Subseafloor hydrothermal circulation drives biogeochemical exchange between the solid Earth and its ocean, and could play a similar role in other ocean worlds. We assess the scale of subseafloor temperature (T) variations during hydrothermal circulation in ~3.5 Ma seafloor on the eastern flank of Juan de Fuca Ridge. This well-studied, moderate T system (~65°C–70°C in the upper ocean crust) represents a warm end-member on Earth, with slow flow across 10s of kilometers. Modest lateral flow between recharge and discharge sites is accompanied by small-scale convection, resulting in variable local T and flow conditions, even for simple, layered models. The flow and T fields are time-varying, with the magnitudes of subseafloor variation oscillating around quasi-steady conditions. The fractions of the crustal aquifer that are in T ranges relevant to different microbial habitats were calculated. In simulations with discharging fluids at ~70°C, temperatures of 40°C–80°C were found within 65%–90% of the aquifer. The same simulation, run with low gravity appropriate for Europa, has 50%–70% of the aquifer at temperatures of 40°C–80°C, and 30%–50% at $T > 80$°C. Tracking of fluid parcels suggests that fluids can heat and cool at rates of 0.2°C~10°C/1,000 yr due to secondary convection. Geochemical modeling based on these simulations indicates that some nutrients and organic molecules in the fluids for this end-member case could vary in concentration up to an order of magnitude as a consequence of such T variability. These findings highlight implications for variations in water–rock reactions and, hence, a potentially transient nature of habitable subseafloor niches.

Plain Language Summary Subseafloor circulation below Earth's ocean, which heats seawater as it flows through the porous oceanic crust, drives chemical and biological exchange between the rocky interior and the ocean. Low-moderate temperature fluids transport the products of chemical reactions between the rock and fluid, and can deliver nutrients that support microbial life. These fluids can travel long distances in the crust before eventually discharging back into the ocean, supporting microbial life at depth and near the seafloor. This study investigates the magnitude of subseafloor temperature variations that characterize a slow-flow hydrothermal system, based on novel analyses of results from prior computer simulations. Calculations of variations in geochemical and nutrient concentrations, both consequential for microbial growth and abundance, show significant differences in habitability for different hydrothermal species. This particular type of hydrothermal system, which can explain the warm end-member case observed on the young, eastern flank of the Juan de Fuca ridge on Earth, could also occur on small ocean moons such as Europa and Enceladus.

Key Points:

- Indirect flow paths during hydrothermal circulation between inflow and outflow sites can result in spatial and temporal variability of subseafloor temperature
- Simulations of a ridge-flank hydrothermal system predict areas of distinct biogeochemical temperature ranges in a shallow crustal aquifer
- This variability can influence organic chemical and nutrient concentrations, and thus the nature of microbial habitats

Supporting Information:

Supporting Information may be found in the online version of this article.

Correspondence to:

D. K. Blackman,
dkblackm@ucsc.edu

Citation:

Blackman, D. K., Robinson, K., Randolph-Flagg, N., Fisher, A. T., Huber, J. A., German, C. R., & Dickerson, K. L. (2026). Subseafloor temperature variability during ridge-flank hydrothermal circulation: Implications for a moderate-temperature earth system and other ocean worlds. *Geochemistry, Geophysics, Geosystems*, *27*, e2026GC012972. https://doi.org/10.1029/2026GC012972

Received 2 APR 2026
Accepted 8 OCT 2026

Author Contributions:

Conceptualization: Donna K. Blackman
Funding acquisition: Donna K. Blackman, Julie A. Huber, Christopher R. German
Methodology: Donna K. Blackman, Kirt Robinson, Noah Randolph-Flagg
Project administration: Christopher R. German

© 2026 The Author(s). Geochemistry, Geophysics, Geosystems published by Wiley Periodicals LLC on behalf of American Geophysical Union.
This is an open access article under the terms of the Creative Commons Attribution-NonCommercial License, which permits use, distribution and reproduction in any medium, provided the original work is properly cited and is not used for commercial purposes.

1. Introduction

Following the first direct observations of hydrothermal discharge on Earth's seafloor, many studies have investigated, measured, sampled, and modeled these coupled flows of fluids, heat, and solutes (Baker et al., 1991; German et al., 2025; Humphris et al., 1995). Subseafloor fluid flow is thought to extract 20%–25% of Earth's global heat and to have a significant impact on the composition of seawater and global chemical cycles (e.g., Coggon et al., 2025; Elderfield & Schultz, 1996; Hasterok, 2013). While high temperature "black smoker" venting in the axial zones of oceanic spreading centers is visually spectacular and has strong local influence on elemental budgets, low-to-moderate temperature flow on ridge flanks contributes to significantly greater heat and mass exchange on a global scale and generates favorable conditions for microbiological activity (Elderfield &

15252027, 2026, 10, Downloaded from https://agupubs.onlinelibrary.wiley.com/doi/10.1029/2026GC012972, Wiley Online Library on [28/10/2026]. See the Terms and Conditions (https://onlinelibrary.wiley.com/terms-and-conditions) on Wiley Online Library for rules of use; OA articles are governed by the applicable Creative Commons License

Writing – original draft: Donna K. Blackman, Kirt Robinson, Noah Randolph-Flagg, Julie A. Huber
Writing – review & editing: Donna K. Blackman, Kirt Robinson, Noah Randolph-Flagg, Julie A. Huber, Christopher R. German, Kristin L. Dickerson

Schultz, 1996; Johnson & Pruis, 2003; Mottl, 2003; Veirs et al., 2006; Wheat et al., 2004). Ridge flanks generally lack active volcanism and extensional faulting that characterize the axial zones; hydrothermal activity in this setting is driven mainly by lithospheric heat loss as the oceanic plate spreads off axis and ages. Prior numerical studies of ridge flank systems focused on fluid discharge temperatures, flow rates, and conductive seafloor heat flow adjacent to outflow sites (e.g., Hutnak et al., 2006; Kremin et al., 2024; Langseth & Herman, 1981; Lauer et al., 2018; Price et al., 2021), developing simulations that match seafloor measurements. However, the spatial and temporal variability of fluid flow and thermal conditions in the subseafloor corridor between recharge and discharge sites has not received much attention. Here we consider these dynamics in order to assess the possible scales of such variability, which in turn, could impact water–rock exchange, reactions that control mineral stability and chemical kinetics, and microbiological processes along hydrothermal flow paths.

Ridge-flank hydrothermal circulation has been identified based on lateral trends of pore fluid chemistry in sediments overlying volcanic crust, and seafloor heat flux values that deviate from lithospheric cooling predictions (e.g., Baker et al., 1991; Davis et al., 1992; Elderfield et al., 1999). In some cases, a significant fraction of predicted lithospheric heat is missing, suggesting advective extraction, and/or lateral redistribution by local convection (Fisher & Harris, 2010). All of these indicators are consistent with transport mainly in the volcanic upper crust, which is generally orders of magnitude more permeable than overlying marine sediments and underlying intrusive rocks (e.g., Fisher et al., 2014; Norvell et al., 2023; Spinelli et al., 2004). Local variations in both heat flux and pore fluid chemistry have helped to locate recharge sites on ridge flanks, with rapid fluid flow into volcanic outcrops such as seamounts (Figure 1; e.g., Fisher et al., 2003; Hutnak et al., 2008; Wheat et al., 2013). Volcanic outcrops allow recharging fluids to bypass low-permeability sediments and then mix and flow laterally in underlying volcanic rocks. Ridge-flank hydrothermal systems operate across a range of thermal and corresponding chemical conditions. Based on P and Mg concentrations of pore fluid samples recovered near the sediment-basement interface in seafloor boreholes, reaction temperatures in these systems are often in the range ∼2°C–65°C (Fisher & Wheat, 2010). Factoring in constraints from O-isotopes in carbonate alteration minerals deposited during seawater circulation, Coogan and Gillis (2018a) infer that there are probably two classes of flank systems—moderate temperature (25°C–70°C) systems that have been found only in crust <15 Myr old, and low temperature systems (5°C–20°C) that have been observed at many more sites and across the full range of plate ages in the modern ocean (and older ophiolites, e.g., Coogan & Gillis, 2018b).

The permeability of volcanic ocean crust can be quite heterogeneous (e.g., Fisher et al., 2014) and there is no direct way to characterize it over multi-km extents of flank hydrothermal systems. Assessments of effective permeability over multi-km length scales come from analytical and numerical calculations (e.g., Davis et al., 2000; Winslow et al., 2016), but these cannot resolve smaller scale spatial variability. In general, volcanic upper crust tends to have high permeability as a result of extrusive construction, accumulation of rubble between lava flows, thermal contraction, and faults (e.g., Clague et al., 2020; Fisher et al., 2014; Haymon et al., 1991; Martin et al., 2007; Tontoni et al., 2016). Permeability in volcanic rocks of the ocean crust has been measured directly in 16 boreholes, yielding a value range of 10^{-17} to 10^{-10} m^2 (Fisher et al., 2014). On ∼6 Myr old Costa Rica ridge flank, results from DSDP Hole 504B indicate a significant permeability decrease ∼600 m below the sediment-basement interface (Anderson et al., 1985). It is clear that fracturing along faults, the majority of which develop within ∼15 km of Pacific spreading axes, creates high permeability zones that can channel seawater flow (Coogan & Gillis, 2018a). Fisher and Becker (2000) invoke a connected network of channels within the shallow crust to enable lateral flow and heat loss that is inferred to occur based on global seafloor heat flow data. However, the occurrence of channelized flow does not preclude coexisting slower flow within intervening, somewhat lower permeability portions of the formation and/or across scales that exceed the extent of the highest permeability zones.

When hydrothermal recharge into one outcrop flows laterally and discharges through another outcrop, this can form a self-sustaining "hydrothermal siphon" (e.g., Fisher & Wheat, 2010; Fisher et al., 2003; Figure 1). This is known to occur between volcanic outcrops separated by tens of km in the eastern Pacific Ocean (e.g., Anderson et al., 2012; Fisher et al., 2003; Hutnak et al., 2008; Le Gal et al., 2018; Villinger et al., 2002). Numerical simulations of ridge flank siphon flow have succeeded in matching inferred discharge rates and surrounding heat flow observations for pairs of basement outcrops on the young (∼3.5 Ma) eastern Juan de Fuca Ridge (JFR) flank (Winslow et al., 2016) and on older seafloor (∼23 Ma) on the eastern flank of the East Pacific Rise (Lauer et al., 2018). Here, we use the hydrothermal system on the JFR flank as a case example. This system is an end-member for ridge-flanks, with modest total fluid throughput (∼5–20 kg/s between two outcrops), localized

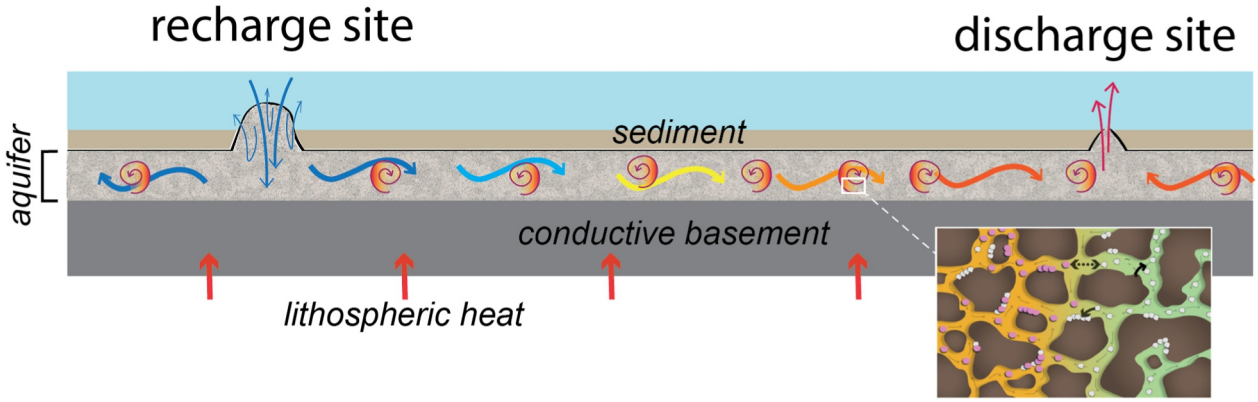


Figure 1. Sketch of a subseafloor hydrothermal siphon showing the main components of the system. At a recharge site, cool ocean-bottom waters enter the permeable crustal aquifer. Some fluids that have absorbed deep-seated heat from the rock formation during flow through the aquifer eventually exit from the discharge site back into the ocean. The flow pattern within the aquifer is often complex and the subseafloor temperature can vary. Local formation temperature affects mineral stability and the rate of the rock reaction with seawater. Such alteration changes local rock composition. Fluid composition evolves too, depending on the formation properties, flow rate, and chemical kinetics (zoom-in box). Flow rates can vary within the aquifer, which also affects the extent of local water–rock exchange and fluid composition.

seafloor thermal signatures, and discharging fluids that are highly altered compared to recharging bottom water (Mottl et al., 1998; Wheat et al., 2004). Nevertheless, this system is probably the best characterized ridge-flank hydrothermal system on Earth, and existing three-dimensional numerical simulations (Winslow and Fisher, 2015; Winslow et al., 2016) allow exploration of variations in subseafloor thermal conditions during transport. In addition, this same system has been used as the basis for the evaluation of subseafloor hydrothermal flow under the low gravity of small ocean worlds elsewhere in the solar system (Fisher et al., 2024). These bodies lack active plate tectonics and volcanism, but they could host hydrothermal systems having temperatures in the range simulated here (Akiba & Fisher, 2025).

A key influence on the present circulation within ~3.5 Ma crust of the eastern Juan de Fuca ridge flank is the rapid sedimentation associated with major riverine input and turbidite flows off the continental shelf (Davis et al., 1992). Several hundred meters of sediment have been deposited on the volcanic basement of the flank, much more rapidly than occurs throughout most of the ocean basins. This results in a conductive boundary layer whose very low permeability precludes thermally significant fluid inflow or discharge, and shifts the persistent seafloor temperature (~2°C) away from the sediment-basement interface. The flow rate from a known discharge outcrop (Baby Bare) is low (5–20 kg/s) and the slow flow allows circulating fluid to heat up along the 50 km corridor connecting it with the Grizzly Bare recharge site (Wheat et al., 2022; Winslow et al., 2016). Borehole-to borehole tracer tests conducted north of Baby Bare confirm that km-scale lateral flow occurs in the shallow basement of this ridge flank (Neira et al., 2016). Chemical signatures document significant rock–seawater exchange at temperatures ~65°C (Wheat and Mottl, 2000), with Ca and Mg concentrations that depart notably from bottom water. While the thick sediment layer is a key feature of the eastern JFR flank, affecting the current thermal regime and the temporal evolution of fluids during circulation, it is not required for recharge and discharge sites to be separated by multi-km distances if ambient seafloor relief is modest away from seamounts and major fault scarps. Indeed, sediment cover 10–20 m thick is sufficient to impede hydrothermal outflow in many settings (e.g., Norvell et al., 2023; Spinelli et al., 2004).

Lateral fluid flow in 3.5 Ma ocean crust on the JFR flank, between the sites of recharge and discharge, is characterized in numerical simulations by mixed circulation, where net lateral transport occurs simultaneously with local convection. These secondary convection cells can be oriented either along the direction of net transport or perpendicular to it (e.g., Kremin et al., 2024; Stein and Fisher, 2003; Winslow and Fisher, 2015). Convective upwelling brings warm fluid to shallow levels within the crustal aquifer, advecting heat toward the seafloor; downwelling transports cool fluid toward the base of the aquifer, reducing ambient temperatures. Simulations indicate that these local convection cells are unstable during mixed circulation, rolling along the aquifer, or breaking up and reforming over time.

In this study, we examine the temporal and spatial variability of simulated temperature fields and flow rates between recharge and discharge sites of a subseafloor hydrothermal siphon. The 3.5 Ma JFR flank system

15252027, 2026, 10, Downloaded from https://agupubs.onlinelibrary.wiley.com/doi/10.1029/2026GC012972, Wiley Online Library on [28/10/2026]. See the Terms and Conditions (https://onlinelibrary.wiley.com/terms-and-conditions) on Wiley Online Library for rules of use; OA articles are governed by the applicable Creative Commons License

15252027, 2026, 10, Downloaded from https://agupubs.onlinelibrary.wiley.com/doi/10.1029/2026GC012972, Wiley Online Library on [28/10/2026]. See the Terms and Conditions (https://onlinelibrary.wiley.com/terms-and-conditions) on Wiley Online Library for rules of use; OA articles are governed by the applicable Creative Commons License

provides the basis for the model geometry and other physical parameters. We subsequently explore how differences in gravity could influence the thermal variability, as might be relevant for other ocean worlds. We consider how fluid compositions might vary in response to the changing physical flow regimes identified. Local temperature and water:rock ratio (the amount of water that circulates through a given amount of rock) affect the nature and rates of chemical reactions (e.g., Coogan & Gillis, 2018a; Elderfield et al., 1999). By directly linking the results of hydrothermal circulation simulations to geochemical modeling, it is possible to assess whether the distributions of certain organic molecules approach metastable abundances and could therefore be diagnostic of subseafloor temperature, pressure, and composition. If so, and as reacting fluids are subsequently discharged, these molecular distributions might serve as tracers of subsurface geochemical processes.

2. Methods

2.1. Hydrothermal Circulation Simulations

We analyze simulations of coupled fluid-heat transport between two outcrops, separated by 50 km, which were developed to test the influence of variations in gravity, heat input, and other properties on flow and temperature conditions (Fisher et al., 2024). Simulations were run using Finite Element Heat and Mass (FEHM), a hydrocode for three-dimensional, time-varying hydrothermal fluid flow and temperature fields. The domain design is based on earlier simulations that successfully replicated several aspects of outcrop-to-outcrop hydrothermal flow within the eastern flank of the JFR (Winslow et al., 2016). The subset of simulations considered here have a 450 m sediment layer overlying a 600 m thick permeable crustal aquifer, with permeability of $\sim 10^{-13}$ to 10^{-12} m^2) overlying a deeper basement that has much lower permeability (10^{-17} m^2). The recharge site is an outcrop with a seafloor surface area of $\sim$1.4 km^2, penetrating through the sediment and separated from a smaller, discharging outcrop with a surface area of 0.14 km^2 (Figure 2a). The aquifer is homogeneous and isotropic, whereas the recharge/discharge features can have permeability that is higher than that in the aquifer, and in some simulations vertical permeability (k) that is 10–100 times higher than horizontal permeability; this is intended to represent higher, or directional, permeability associated with the deposition of rubbly flows, cracking, and subvertical fracturing and old feeder channels within an inactive volcanic structure. Heat flow, specified at the base of the conductive region ($\sim$4–5 km below the seafloor), averages 196 mW/m^2 (Winslow et al., 2016). These are transient simulations, run until quasi-steady flow develops (generally in a few 100 kyr of simulations time) and allowed to continue for an additional 0.5–1.0 Myr; flow and temperature field results were output during this later period. Outputs were triggered numerically based on the passage of a specified number of timesteps. The length of the time step can be adjusted if model flow rates vary significantly (Table S1 in Supporting Information S1). See Fisher et al. (2024) for further details of the numerical model methodology and the full suite of simulations run.

The simulations discussed here (Table 1) include those that (with Earth gravity) produced flow rates and heat output consistent with field data (Fisher et al., 2024; Winslow et al., 2016). A subset of these simulations helps to explore how a few parameter values influence subseafloor temperature variations for an Earth system (simulations Ea-1, Ea-2, and Ea-3). A single Earth case (Ea-4) tests the effect of having an aquifer that is 600 m deeper (and therefore warmer). Two scenarios (Eu-1, Eu-2) test how low gravity (1.3 m/s^2), appropriate for Jupiter's moon Europa, affects the results. Most simulations predict fluid discharge temperatures $T_{dis} = 71$–76°C. The deep aquifer Earth case (Ea-4) discharges fluids at 114°C (at a notably higher flow rate), and the Europa-like gravity case with $k = 10^{-13}$ has T_{dis} of 58°C. The relatively large outcrop at the recharge site, and limited lateral transmissivity within the aquifer result, in a majority of the inflowing fluid circulating locally and returning to discharge through the same site (Winslow and Fisher, 2015; Winslow et al., 2016). Only a fraction of the inflowing seawater at the recharge site gets entrained as siphon flow and eventually exits at the discharge site.

The aquifer layer extends to the edges of the model domain (Figure 2a), but we are most interested in temperature variations of the fluid that may eventually be released into the overlying ocean from the discharging end of the siphon, where a discernible redox gradient and/or other biogeochemical signatures might be observable. The recharge–discharge site geometry results in an overall dipolar circulation pattern. Analytic dipole solutions for paired recharging and discharging groundwater wells predict that 50% of the flow occurs within a circle of diameter equal to the distance between the two sites and centered at the midpoint between them (Haitjema, 1995). Therefore, we choose a centered, cylindrical region, extending from the base to the top of the aquifer, to assess temperature variations that occur within the subseafloor (Figure S1 in Supporting Information S1). We calculate the fraction of this cylinder for which temperature is predicted to fall within four ranges that are relevant for

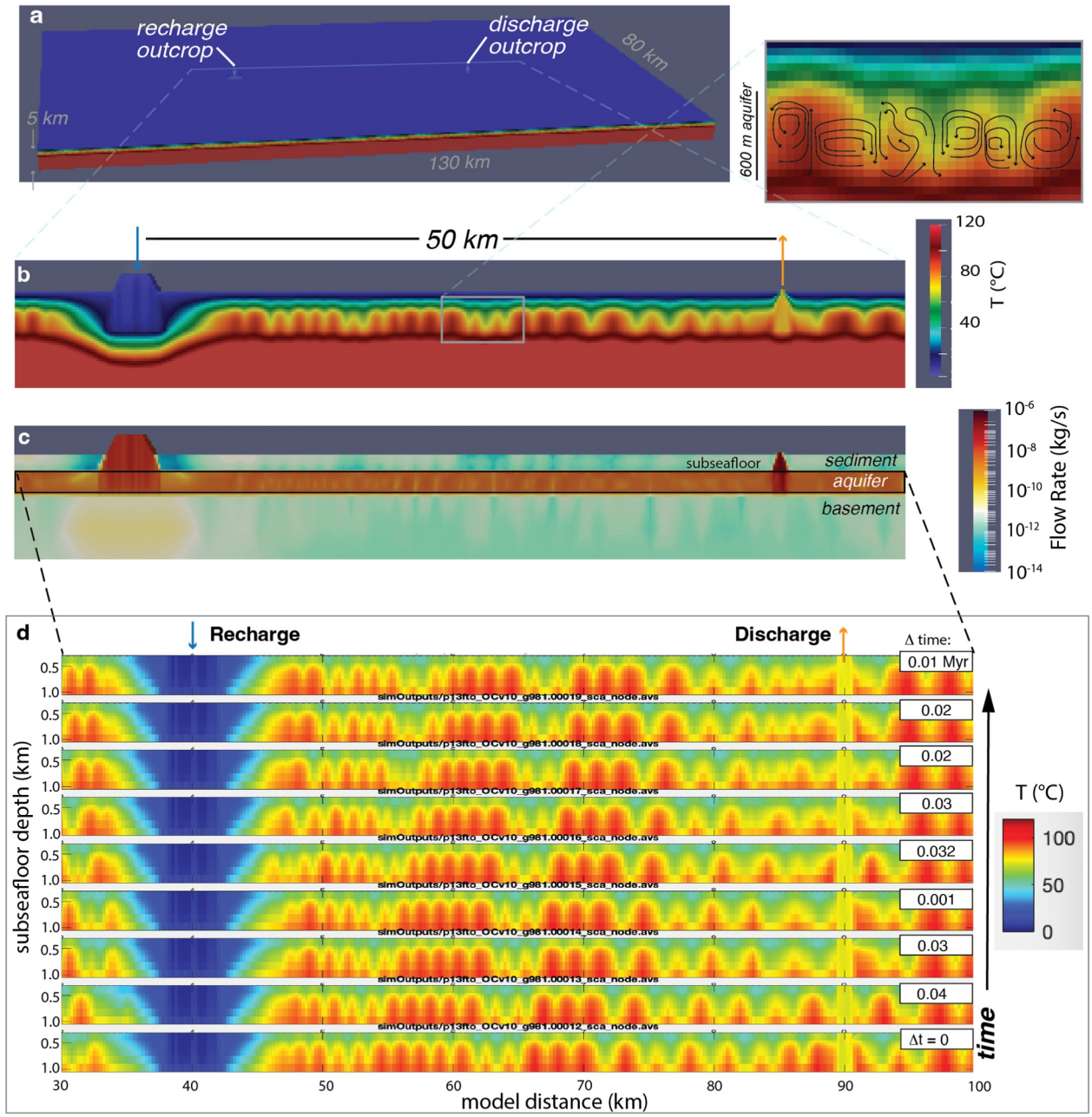


Figure 2. Cross-section of 3-D seafloor hydrothermal siphon model and results for Ea-2. (a) Full model geometry, with color showing temperatures *(T)* after dynamic steady state is achieved. (b) *T* profile between recharge and discharge sites (VE = 3X). The zoomed-in box depicts computed convective flow and how it corresponds to local *T*. (c) Fluid flux (total magnitude) for the same profile. (d) Time variation of *T* within the aquifer portion of the profile for snapshots in time (VE = 4X). The time elapsed between each panel and the one below is labeled in the upper right. Convective rolls visible in (b) migrate from recharge to discharge site over time, but the range of *T* variation within the aquifer is consistent once the model reaches dynamic steady state.

microbial habitability: T = 0°C–40°C (psychrophile and mesophile compatible); 40°C–80°C (thermophiles); 80°–120° (hyperthermophiles); and >120°C (at or above the widely accepted upper limit for viability of life on Earth; Takai et al., 2008). The fraction of the cylindrical region of interest that falls into each of the temperature ranges differs by less than 1% between all the runtimes evaluated for each of the simulations (Table S1 in Supporting Information S1).

Mapping the pathways of fluid parcels in the subseafloor was accomplished with post-simulation particle tracking, based on a synoptic assessment of the fluid flow field (e.g., Pollock, 2016; Schröder and Schanz, 2023).

15252027, 2026, 10, Downloaded from https://agupubs.onlinelibrary.wiley.com/doi/10.1029/2026GC012972, Wiley Online Library on [28/10/2026]. See the Terms and Conditions (https://onlinelibrary.wiley.com/terms-and-conditions) on Wiley Online Library for rules of use; OA articles are governed by the applicable Creative Commons License

15252027, 2026, 10, Downloaded from https://agupubs.onlinelibrary.wiley.com/doi/10.1029/2026GC012972, Wiley Online Library on [28/10/2026]. See the Terms and Conditions (https://onlinelibrary.wiley.com/terms-and-conditions) on Wiley Online Library for rules of use; OA articles are governed by the applicable Creative Commons License

Table 1
Model Parameters and Portion of Subseafloor Aquifer in Different Temperature Ranges

Simulation	Aquifer k (m^2)	Outcrop k (m^2)	Discharge rate (kg/s)	T_{dis} (°C)	$T_{aq} < 40$ (°C)	$40 < T_{aq} < 80$ (°C)	$80 \leq T_{aq} < 120$ (°C)	$T_{aq} > 120$ (°C)
Ea-1	10^{-12}	10^{-10}	150	71.6	9%	88%	3%	0%
Ea-2	10^{-13}	10^{-10}	21	72.6	3	66	31	0
Ea-3	10^{-13}	10^{-12}	19	72.2	3	65	32	0
Ea-4[a]	10^{-12}	10^{-10}	600	114	27	33	38	2
Eu-1	10^{-12}	10^{-10}	28	76.8	2	69	29	0
Eu-2	10^{-13}	10^{-10}	1.5	58.1	1	50	43	6

Note. k is permeability, aquifer is 600 m thick, and basal heat flow is 196 mW/m^2. All discharge temperatures (T_{dis}) and flow rates are from Fisher et al. (2024). Ea-3 has parameters favored by Winslow et al. (2016) for Juan de Fuca ridge flank. Gravity for Earth simulations (Ea-1 through Ea-4) is 9.81 m/s^2; for Europa-like models (Eu-1 and Eu-2) it is 1.3 m/s^2. [a]Ea-4 has an aquifer 600 m deeper than other simulations, with the top at 1050 m subseafloor instead of 450 m.

Flow-paths were computed for models Ea-1, Ea-2, Ea-4, and Eu-1, by forward- and back-tracking fluid parcels within the velocity field after it reached a dynamic steady state. Results reported here emphasize fluid paths in the corridor extending from recharge to discharge sites. FEHM results were imported into ParaView (https://www.paraview.org/) and the StreamTracer algorithm was employed using Runge-Kutta integration and a 100-point cloud within a sphere of radius 2.5 km, centered just inboard (toward the opposite site) of either the recharge (forward tracking) or discharge site (backtracking). Time along the fluid parcel path, temperature (T_f), and flow rate of the fluid parcels were output for each position along their respective flowpaths (please see additional explanation in Supporting Information S1).

2.2. Linked Calculations of Geochemical Variability

The temporal and spatial variations in the temperature of fluid parcels flowing along the aquifer can affect their nutrient concentrations and organic molecule reactions. In hydrothermal systems, the concentrations of some organic compounds vary in response to differences in system T, pressure, pH, and redox state (Cruse & Seewald, 2006; Helgeson et al., 1993; McDermott et al., 2015; Seewald et al., 2024; Shock, 1988, 1989; Tassi et al., 2007). Experiments show in greater detail how various sets of organic compounds react to approach metastable equilibrium abundances that are controlled by these same parameters (Robinson et al., 2020, 2021a, 2023, 2024, 2026; Seewald, 1994, 2001). By linking the T evolution of individual fluid parcels directly to a geochemical model, we can assess the nature of possible variations. Time, local temperature, and/or local flow rate of the parcel are input to each geochemical model, with computed fluid chemistry evolving based on these (and other) conditions, using the following approach for nutrients and organic compounds.

Variation in the concentration of nutrients within a fluid parcel is assessed following the method developed by Randolph-Flagg et al. (2023). To obtain some quantitative constraint on P concentrations that could occur in hydrothermal fluids on Enceladus, these authors conducted millions of chemistry simulations for a wide range of assumed T, chondrite composition, and water rock ratio. For the present study, the approach is extended to other species—C, Ca, Mg, Fe, and S. The extent of reaction between hydrothermal fluid and wallrock at each position and corresponding T is predicted with EQ3/6 modeling (Wolery, 2010), for the end-member scenario where local equilibrium is reached. To illustrate the possible scale of nutrient variation within a fluid parcel for this study, we consider a single scenario assuming carbonaceous chondrite rock composition (CI) and specify a low water:rock mass ratio of 0.1.

To assess the use of organic molecules as tracers of fluid parcel evolution, we consider the approach to equilibrium of ammonia, amines, and alcohols. In experiments focused on methylamine or benzylamine, steady state abundances are achieved and are strongly affected by both T and pH (Robinson et al., 2020, 2024, 2026). Notably, there is evidence that suggests these "model" experimental compounds may be present in small ocean worlds (Section 4.3). Here, we combine T and flow rate predictions from the hydrothermal simulations with previously determined chemical kinetics (Robinson, Gould, et al., 2021) and thermodynamic property data (Robinson et al., 2024) to predict whether benzylamine, benzyl alcohol, and ammonia would approach steady state abundances reflective of temperature. T-dependent rates generated from 200°C to 300°C experiments on benzylamine

15252027, 2026, 10, Downloaded from https://agupubs.onlinelibrary.wiley.com/doi/10.1029/2026GC012972, Wiley Online Library on [28/10/2026]. See the Terms and Conditions (https://onlinelibrary.wiley.com/terms-and-conditions) on Wiley Online Library for rules of use; OA articles are governed by the applicable Creative Commons License

deamination (Robinson, Gould, et al., 2021) were combined with thermodynamic estimation strategies to calculate reverse reaction rates (Robinson et al., 2024). More details can be found in Supporting Information S1, but in brief, we used both temperature-dependent reaction rate constants experimentally derived from Arrhenius relationships, and temperature-dependent equilibrium constants calculated using thermodynamic software (Boyer, 2024; Dick, 2019) to model reversible chemical reaction kinetics. This has allowed us to predict whether the selected compounds would approach relative abundances reflective of system temperature along a given fluid parcel path.

3. Results

We report the results of temperature analyses for the rock formation within the aquifer and several representative fluid parcels tracked through different model velocity fields (Section 3.1). We describe the results of selected geochemical calculations to illustrate the scale of biologically relevant geochemical variations that correspond to the determined temperature evolution (Section 3.2).

3.1. Physical Predictions for Aquifer Formation and Fluid Temperatures

For the simulations examined, the distribution of formation temperatures within the subseafloor aquifer can differ considerably between the models tested, despite their having similar discharge temperatures (T_{dis} ~72°C). At any location in the aquifer, temperature increases and decreases repeatedly over time as convective cells roll by, with warm fluid rising and cooler fluid sinking. Not all portions of fluid flow paths cycle across the full depth extent of the crustal aquifer; some fluid parcels circulate across a more limited depth interval. Fluid tends to move faster in larger convective rolls, attaining greater buoyancy due to higher temperature reached near the base of the aquifer. Smaller convective cells do not reach the aquifer base/top, and fluid does not heat/cool as much, resulting in lower upwelling/downwelling rates. Specifics of the results are provided below, in Figures 2 and 3, and in Supporting Information S1.

The Earth models with a shallow aquifer (Ea-1, Ea-2, and Ea-3) all show a majority (65%–90%) of the cylindrical portion of the aquifer formation having temperature "T_x" = 40°C–80°C, a small fraction (3%–9%) having T_x < 40°C, and the remainder (3%–31%) at T_x = 80–120°C (Table 1). Flow rates are greater for the higher permeability case (Ea-1, aquifer $k = 10^{-12}$ m^2), and thus more heat is advected and a smaller fraction of the subseafloor reaches T_x > 80°C. The Earth model with a deeper aquifer (Ea-4), has a higher T_{dis} ~ 114°C and the discharge rate is considerably higher than the shallow aquifer simulations. This is due to the higher pressure differential between the cold recharge site and the warm discharge site. The T_x field for Ea-4 is also more evenly distributed between the three main temperature bins, with ~2% rising above 120°C (Table 1). In this case, there is a tradeoff between greater ambient temperatures at the increased depth and higher transport rate, which results in 27% of the cylindrical region having T_x < 40°C, and 33% and 38% in the 40°C–80°C and 80°C–120°C bins, respectively (Table 1).

The scale of the temperature oscillations at a given model location between the model output runtimes is ±15°C for the higher permeability, shallow aquifer Earth case (Ea-1) and greater for lower permeability or deep aquifer cases (±20°C–30°C, Ea-2, Ea-3, and Ea-4) as well as the higher permeability Europa case (Eu-1) (Figure S2, Table S1 in Supporting Information S1). Although the T_x change depends on the timestep considered, the consistency of values across all snapshots and timesteps considered indicates that they reliably represent the magnitude of variations over time. Comparing rates of T_x change (dT_x/dt) is also illuminating: Most simulations dT_x/dt rates range from 0.2°C to 0.8°C/1,000 yr (Table S1 in Supporting Information S1). The exception is the lower permeability Europa gravity case (Eu-2) for which dT_x/dt is typically 0.05°C–0.07°C/1,000 yr.

We also analyzed a low heat-input case that employs all the same parameters as Ea-4 except that basal heat flow is 49 mW/m^2, corresponding to a plate age of ~100 Myr. Secondary convection again develops, resulting in lateral temperature variability of ±7°C (vs. up to ±30°C with basal heat of 196 mW/m^2, Table S1, Figure S2 in Supporting Information S1). As expected, the aquifer is cooler overall than for Ea-4, with ~90% of the circular region between recharge and discharge below 40°C and ~10% in the range 40°C–80°C. The discharge fluid temperature is 35°C and flow rate is 150 kg/s. The main point here is that subseafloor temperature variability can persist in subseafloor hydrothermal systems for which there is low heat input (equivalent to some of Earth's oldest seafloor).

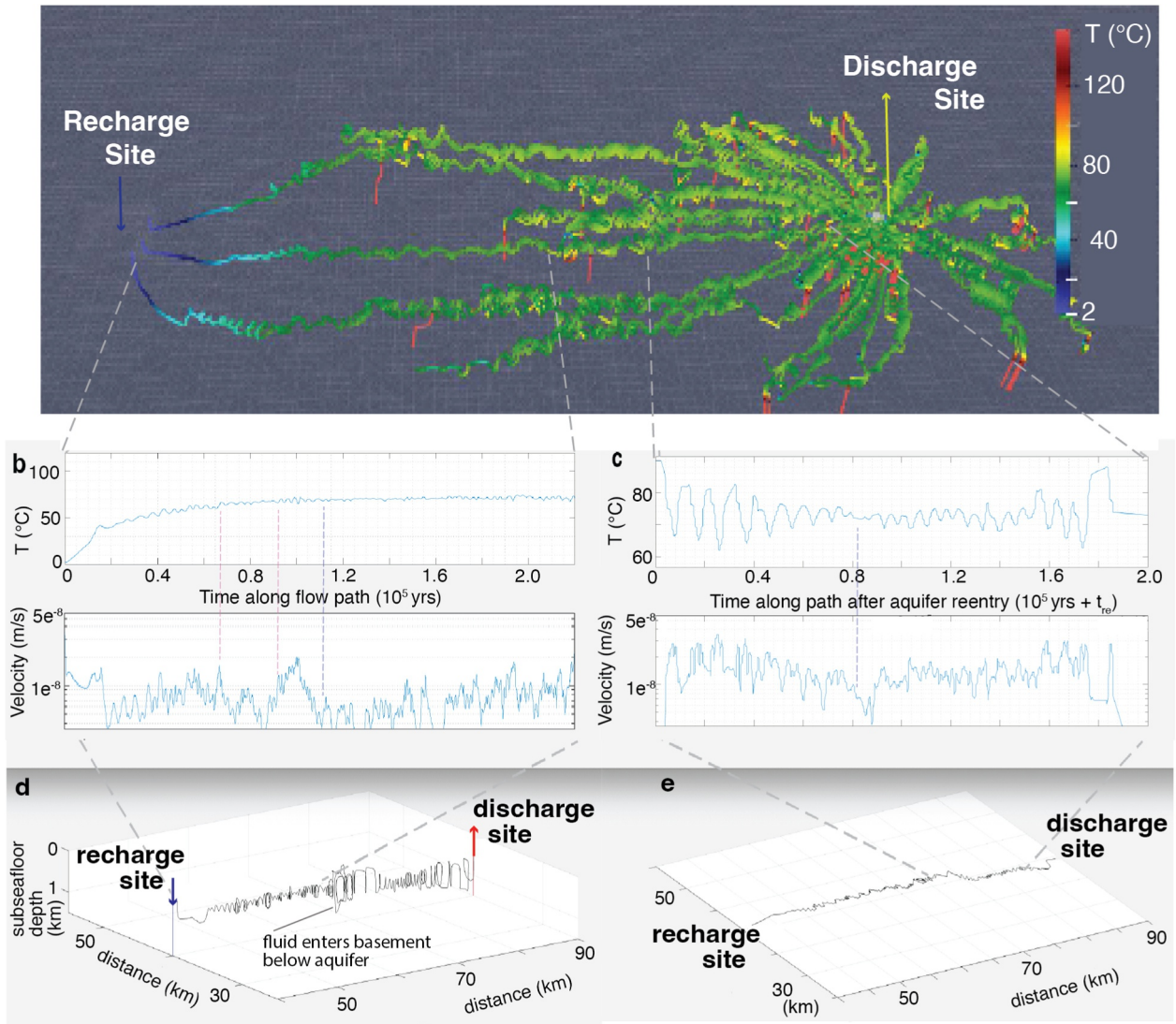


Figure 3. Evolution of temperature and velocity along the paths that fluid parcels travel in model Ea-2. Paths calculated for the flow field at the final time step. (a) Temperature (T_f) evolution for several fluid parcel paths. Color scale differs from Figure 2 to highlight the temperature increase of parcels that travel a very short portion of the path in the basement below the aquifer. (b, c) each show fluid evolution along a portion of a single parcel path, with T_f plotted in upper panels and fluid velocity in lower panels. Note that T scales differ between (b) and (c). Panels (d) and (e) show the full streamline in 3-D and mapview, respectively, portions of which are shown in panels (b) and (c). The fluid velocity slows significantly when the parcel enters the low permeability basement underlying the aquifer, near the midpoint of the streamline. Thus, there is a large time offset between the end of the portion shown in (b) and the start time of the portion shown in (c). Fluid flow rate increases when the parcel heats up near/within the basement and rises back into the permeable aquifer, as highlighted by dashed vertical lines in panels (b) and (c).

The rate of temperature change for fluid parcels (T_f) as they convect along the recharge–discharge corridor can be considerably greater than the rate of temperature change at specific locations in the rock formation (Figure 3). T_f continuously varies at different rates along different portions of each parcel flow path (Figures 3b and 3c; Figures S3a, S3b, and S4a in Supporting Information S1). While mean dT_f/dt rates can be low (fraction of a °C/1,000 yr, Figure S3b in Supporting Information S1) when considered over a full flowpath, it is common for rates to range up to 5–10°C/1,000 yr for periods of a few thousands of years (Figure S3 in Supporting Information S1).

Along-path fluid flow rates (Figure 3b) range from 0.5 to 6 m/yr for models with higher permeability ($k = 10^{-12}$), and the lower permeability cases have flow rates commensurately lower. For flowpaths that stay within a ~20 km wide corridor connecting the recharge and discharge sites, flow rates can reach 2–4 times the rates seen elsewhere in the aquifer. Fluid parcels mainly travel within the aquifer , but since both the underlying basement and the overlying sediments have finite (albeit low) permeability, flow paths can result in fluid parcels being transported

15252027, 2026, 10, Downloaded from https://agupubs.onlinelibrary.wiley.com/doi/10.1029/2026GC012972, Wiley Online Library on [28/10/2026]. See the Terms and Conditions (https://onlinelibrary.wiley.com/terms-and-conditions) on Wiley Online Library for rules of use; OA articles are governed by the applicable Creative Commons License

15252027, 2026, 10, Downloaded from https://agupubs.onlinelibrary.wiley.com/doi/10.1029/2026GC012972, Wiley Online Library on [28/10/2026]. See the Terms and Conditions (https://onlinelibrary.wiley.com/terms-and-conditions) on Wiley Online Library for rules of use; OA articles are governed by the applicable Creative Commons License

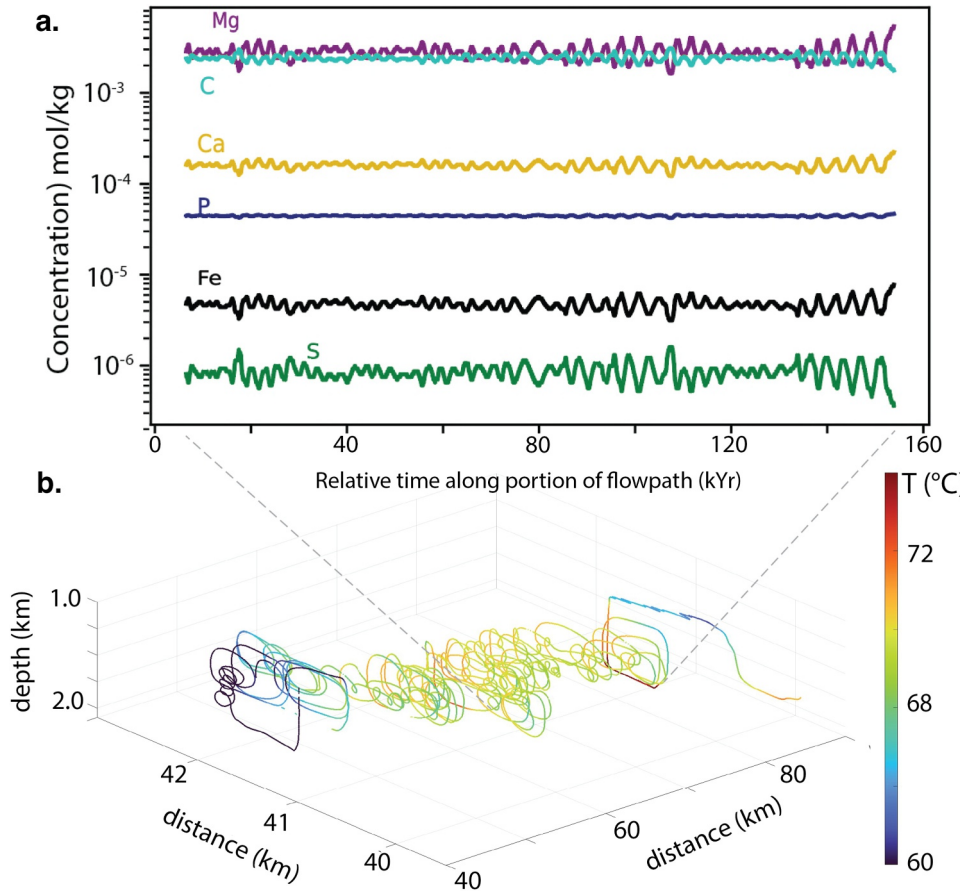


Figure 4. Nutrient concentration variations that correspond (solely) to evolving T_f as a fluid parcel flows along a path in simulation Ea-1. (a) Concentrations obtained using the method of Randolph-Flagg et al. (2023). Note that S and C vary with opposite phases from Fe, Mg, and Ca, in part due to carbonate precipitation. (b) Path of this fluid parcel from recharge to discharge site; color shows temperature. Buoyantly rising fluid is warmer than downwelling fluid.

above or below the main aquifer (Figure 3d; Figure S3 in Supporting Information S1). Flow rates outside the aquifer, where permeabilities are set to $\sim 10^{-17}$ m^2, are very slow, so fluid may spend tens of thousands of years there before possibly returning to the aquifer. This behavior was determined for some of the flowpaths calculated. Here, we focus on characteristics only within the aquifer portion of a parcel's evolution since it captures the behavior within the dominating siphon flow.

3.2. Examples for Scale of Corresponding Geochemical Predictions

Essential nutrients for life such as phosphate, sulfur, and carbon and the micronutrient Fe may become available (or sequestered) as they transition through the subseafloor under temperature and water:rock ratio ranges calculated in these hydrothermal simulations. For a case where the water:rock ratio is 0.1 and the rock composition is that of CI chondrites, the ±2–12°C temperature variations within the aquifer of simulation Ea-1 correspond to [Ca] variations of a factor of 2, whereas [S] varies by nearly an order of magnitude. [P] and [C] are nearly constant, whereas [Mg] and [Fe] vary by a factor of 4 (Figure 4). The relatively modest predicted changes in these solute concentrations have implications for aquatic cell abundance and growth rate. Much larger changes in chemistry would be predicted across the full range of temperature experienced during passage through this hydrothermal system, including deviations from bottom water of 50°C–60°C within much of the aquifer and up to 100°C below the site of seafloor discharge.

To assess potential changes in organic chemistry as fluids flow along the subseafloor corridor, we consider a single flow path through model Ea-4 (Figure S5 in Supporting Information S1) and reactions between a suite of compounds—ammonia, amines, and alcohols. Initially, after fluids infiltrate the seafloor and begin to move along

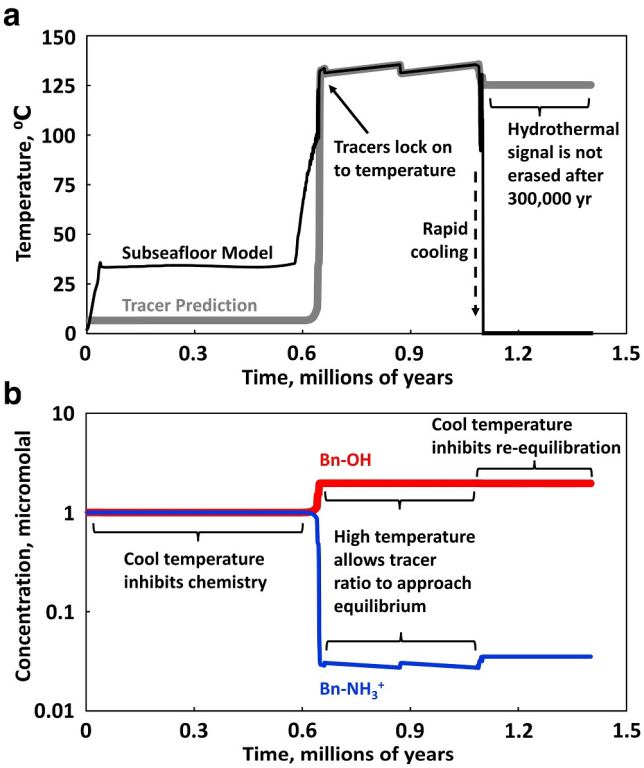


Figure 5. Tracer response to T variability in simulation Ea-4. (a) Evolution of fluid parcel T_f along a flowpath from recharge to discharge site (black line); corresponding organic tracer evolution (gray line). Despite rapid cooling when the fluid discharges (~1.1 Myr along flowpath), the organic tracer exhibits a signature diagnostic of high subseafloor T_f. (b) Changes in concentration of the individual molecules whose ratio-dependent T prediction is shown in (a), based on T-dependent reaction rates and the T_f evolution determined for this flowpath. Red curve shows benzyl alcohol (Bn-OH); blue shows benzylaminum (Bn-NH_3^+), the protonated form of benzyl-amine, which is dominant across most environmental pH values.

the recharge–discharge corridor, reaction rates are slow due to low temperatures (~35°C), but reactions are rapid once temperatures exceed 125°C and the tracers quickly lock on to simulated local conditions. Our kinetic model (detailed in Text S1 of Supporting Information S1) reveals a suite of possible thermal histories that would allow this set of potential tracers to respond to different reactive conditions—for example, 0.5 Myr at 95°C or ~1,000 yr at 145°C (Figure S7 in Supporting Information S1). Fluid parcel tracking from simulation Ea-4 (Figure 5) linked to reaction calculations (Figure 5) also predicts that if the tracers are quickly cooled to bottom seawater temperatures (as would occur during rapid ascent from below the discharge site), they would preserve the hydrothermal signal indefinitely because their reaction chemistry becomes too sluggish at near-freezing temperatures to alter the molecular abundance ratios established at higher temperatures.

The application of this method for the Ea-4 simulation, for which reaction temperatures are higher than other models considered here, allows us to illustrate the principle of using organic molecule tracers to assess subseafloor conditions, since the benzylamine system is well characterized and it responds strongly in this T range. Section 4.2 briefly discusses other systems that the initial work suggests would also respond at lower T.

4. Discussion

In this section, we discuss findings based mainly on the nature of temperature variability, alone. We are aware that both geochemical and microbiological processes could lead to temperature feedbacks, thereby influencing fluid/rock evolution, for example, by causing changes in hydrogeologic properties. However, by isolating the influence of the temperature and flow rate variations first, we aim to provide an indication of the magnitude of associated geochemical (Section 4.1) and biological (Section 4.2) responses that are expected. The potential relevance to ocean worlds beyond Earth is the topic covered in Section 4.3. Section 4.4 catalogs the limitations of this approach and suggests some next steps for building toward fully reactive simulations.

4.1. Implications for Geochemistry

Geochemical exchange associated with marine hydrothermal circulation is a key means for materials to cycle between the solid and fluid spheres of the Earth system (Coggon et al., 2025; Elderfield & Schultz, 1996; Humphris et al., 1995). Temperature can act as a major control on both the rate and the extent of chemical reaction between seawater and rock of the ocean crust, as well as the mineral alteration and dissolution products that result. Water:rock ratios and the compositions of both the reacting fluid (evolved from seawater) and the host rock also play important roles. All of these factors influence the type and amount of chemical species released during reaction at any given location along the hydrothermal flow trajectory, with important implications for the chemical energy potentially available for microbial metabolism. Hydrogen offers a well-studied example. H_2 is a potent energy source for chemolithoautotrophic microbes, and its production during water:rock reaction is a function of both temperature and rock composition (Amend et al., 2011). Temperature variation alone, within the range emphasized here (10°C–120°C), can result in 1-2 orders of magnitude difference in H_2 production (Bach, 2016; Ely et al., 2023), including differences that influence hydrothermal systems in which microbes are known to utilize H_2 metabolically (Reveillaud et al., 2015).

It is notable that modest temperature variations (±<15°C for case Ea-1, discussed in Section 3.2) could also impact relative nutrient concentrations within hydrothermal fluids, with implications for microbial habitability. Any variation in the mix of "reactant" species could impact the amount of chemical energy released and hence local cell abundances and growth rates, whether at fixed locations within the crustal aquifer or in mobile parcels of fluid moving through the aquifer (Figure 1, inset). Previous work on subseafloor microbial communities in

15252027, 2026, 10, Downloaded from https://agupubs.onlinelibrary.wiley.com/doi/10.1029/2026GC012972, Wiley Online Library on [28/10/2026]. See the Terms and Conditions (https://onlinelibrary.wiley.com/terms-and-conditions) on Wiley Online Library for rules of use; OA articles are governed by the applicable Creative Commons License

15252027, 2026, 10, Downloaded from https://agupubs.onlinelibrary.wiley.com/doi/10.1029/2026GC012972, Wiley Online Library on [28/10/2026]. See the Terms and Conditions (https://onlinelibrary.wiley.com/terms-and-conditions) on Wiley Online Library for rules of use; OA articles are governed by the applicable Creative Commons License

venting fluids from the Mid-Cayman Rise, for example, has already indicated that low phosphate conditions exert an important selective pressure on one genus of vent bacteria, with nutrient limitation driving microbial adaptation in the subseafloor (Moulana et al., 2020). While the illustrative calculations shown here (Figure 4) are based on full chemical equilibration, an extreme case in which there would be no energy available for organism use, disequilibrium may be more common in natural systems, at least partly as a consequence of changes in parcel T_f (thus local reaction T) and/or flow rate during transport. Notably in Earth systems, heterogeneity in pore structure and anisotropic permeability produce pore scale fluid mixing that is not resolvable at the simulation scales applied in the present study (e.g., Lee et al., 2025).

The simulations of coupled flow and T in the subseafloor presented here illustrate that fluid temperature and the associated duration of conditions could be sufficient for classes of organic compounds to reach abundances that could be measured to deduce reaction conditions. We find that this approach could be feasible for amines, alcohols, and ammonia. If a similar approach works for other reactions, such as the ethanol-ethene system as suggested in a recent study (Robinson et al., 2023), there may be a suite of viable organic molecular tracers that, together, could provide useful constraints from exiting fluid compositions on the physical regime within the underlying aquifer in low-moderate T hydrothermal systems.

4.2. Implications for Microbial Metabolisms

The temperature ranges and variability characterized in the shallow, subseafloor aquifer reported in this study correspond generally to the type of microbial life that could live in each respective temperature range: mesophiles15°C–45°C; thermophiles 41°C–79°C, and hyperthermophiles >80°C. Our finding that the majority of the model aquifer falls in the 40°–80° range suggests that thermophiles might be the best adapted to life in a moderate temperature subseafloor aquifer, from a purely physical perspective, under the simulated thermal and hydrogeologic conditions. However, at lower effective aquifer permeability (10^{-13} vs. 10^{-12} m^2), a significant portion (~35%) of the aquifer would overlap with the growth optimum range for hyperthermophiles. A very small portion of the deep aquifer Earth model (Ea4) would be expected to reach temperatures at and beyond the known limits to life on Earth ($T > 120$°C). This occurs only on the periphery of the cylindrical region on one side of the discharge site; most fluid flowing from the recharge site would not transit through this basal edge of the cylindrical region prior to exiting at the seafloor. Since the discovery of deep-sea hydrothermal vents and over the subsequent decades, it has been noted that microbial communities investigated in samples of fluids venting from the seafloor along oceanic spreading centers span a wide temperature range of growth, resulting from the highly variable mixing regimes between cold, oxidized seawater and hot, highly reduced hydrothermal fluids that occur in the subsurface (Fortunato et al., 2018; Huber & Holden, 2008; Jannasch & Mottl, 1985). Much less is known about microbial communities in the aquifer of ridge flanks such as those modeled here, with the exception of the Juan de Fuca ridge flank subseafloor microbial community, which has been relatively well characterized. Recent studies indicate that these flank fluids are dominated by a low-biomass, low diversity community of anaerobic thermophiles carrying out sulfate reduction and methane cycling (e.g., Junbluth et al., 2016; Lever et al., 2013; Robador et al., 2015). Variability in temperature plays an essential role in microbial activity, including an organism's ability to synthesize Adenosine TriPhosphate, for example (Hoehler, 2004).

Robador et al. (2015) incubated fluids from the Juan de Fuca Ridge flank over a range of temperatures to measure sulfate reduction rates and found co-existing mesophilic and thermophilic groups of sulfate reducers, consistent with model results that have different portions of the same subseafloor aquifer experience different temperatures at the same time, whether at different depths within that aquifer or due to advective fluid flow. Those authors also found that sulfate reduction was limited by the decreasing availability of organic electron donors at higher temperatures, meaning that as temperature increased, energetic constraints made the metabolism studied more challenging (Robador et al., 2015). Applying results from the present study, we might infer that mesophilic and thermophilic variants would be better adapted to conditions at different places/times in the subseafloor domain, with the ~10 km wide region around the recharge site favoring the lower temperature forms, if physical factors dominate their selection.

4.3. Implications for Other Ocean Worlds

The discovery of oceans on several solar system moons suggests the likelihood of geochemical exchange between their seawater and rocky interiors (Nimmo & Pappalardo, 2016), with the potential to establish redox disequilibria

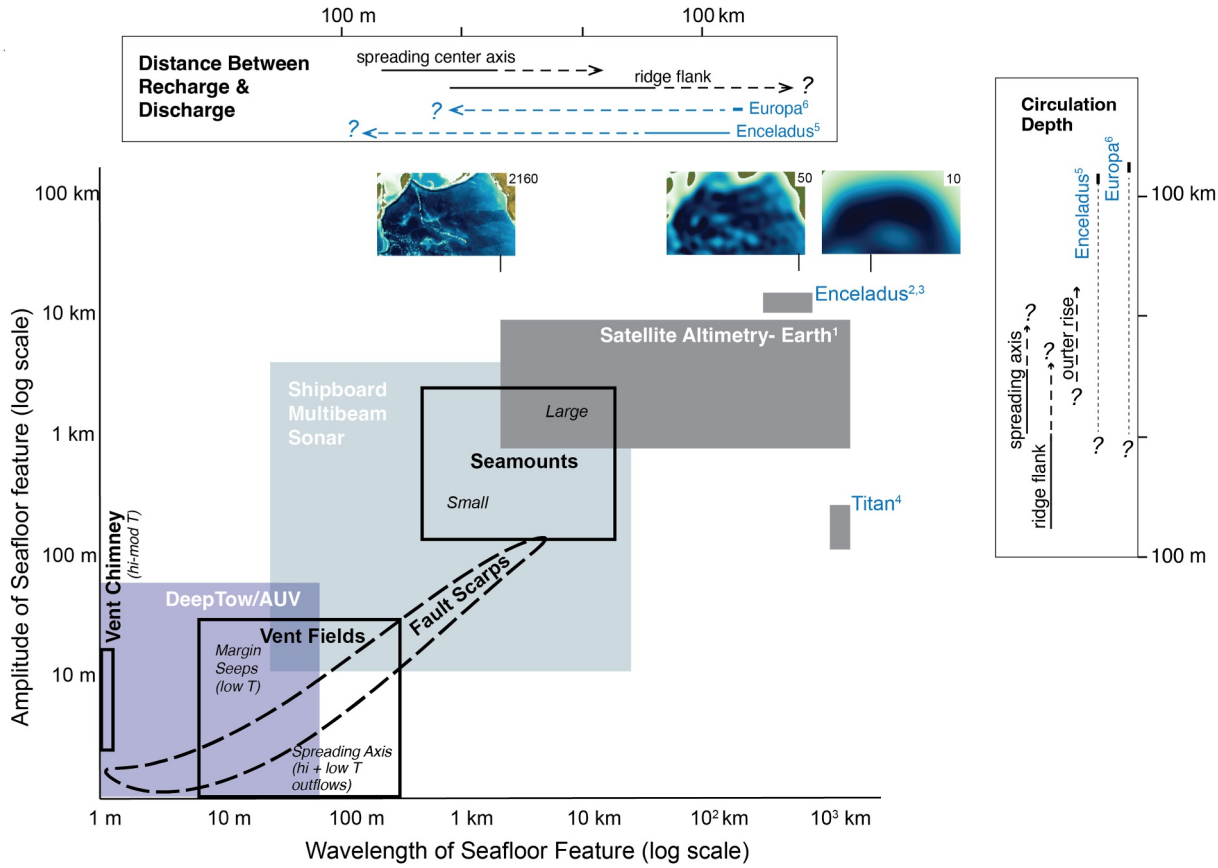


Figure 6. Spatial scales of seafloor features and fluid circulation in hydrothermal systems. The main diagram depicts the scale of seafloor features on Earth (black outlined boxes), and current data resolution for Earth and other ocean worlds, for various measurement tools (shaded boxes, white labels). Dashed fault scarp scale region on the main diagram is a rough indication. *T*: temperature, *low*: <80°C; AUV: autonomous underwater vehicle. (1) Sandwell et al., 2014; (2) McKinnon, 2013; (3) Hemingway and Mittal, 2019; (4) Cadek et al., 2021. Color images along the top show Pacific seafloor relief at 3 different spherical harmonic representations (labeled in upper right corner; modified from Salaree & Okal, 2020). Boxed diagrams outside the main plot illustrate the scale of lateral offset between recharge and discharge sites (above) and the depth of hydrothermal circulation (at right). In these boxes, lateral/vertical length scale estimates are: From global ocean world thermal/flow models (blue lettering, (5) Choblet et al., 2017; (6) Travis et al., 2012); inferred from Earth observations (black lettering) of micro-seismicity patterns (Tolstoy et al., 2008), vent fluid temperature, chemistry and chimney distributions (Delaney et al., 1997; Haymon et al., 1991), seismic imaging/anisotropy (Carbotte et al., 2012; Dunn & Forsyth, 2003; Miller et al., 2020), and numerical modeling (Fisher et al., 2024; Lauer et al., 2018; Winslow et al., 2016; Winslow and Fisher, 2015).

that could be exploited by microbial metabolism (Hand & German, 2018). Initial studies modeled hydrothermal circulation in the interior of Enceladus and Europa at a global scale (e.g., Choblet et al., 2017; Travis et al., 2012) and/or assumed radially symmetric, homogeneous layers making up the rocky interior (e.g., Vance et al., 2007). Those contributions provide a plausible basis for advective and reactive processes, but not the only sets of relevant conditions. Experience exploring Earth's seafloor systems shows that local to regional variations in properties and morphology control hydrothermal flows and related processes. Recent modeling has explored more local flow scenarios to assess how lower gravity and/or internal heating (compared to Earth) could result in sustainable (long-term) subseafloor hydrothermal circulation below the seafloor of other ocean worlds (Akiba & Fisher, 2025; Dickerson et al., 2025; Fisher et al., 2024).

Seafloor features that channel off-axis hydrothermal circulation on Earth include seamounts and other volcanic structures or fault scarps having relief amplitudes from tens of meters to several kilometers, and wavelengths of a few to several kilometers (Figure 6). On other ocean worlds, there is almost no constraint on what the character of the seafloor might be, beyond it having a silicate composition (Schubert et al., 2004), that is possibly hydrously altered (Malamud & Prialnik, 2013; Vance et al., 2007; Zandenel et al., 2021), and possibly covered with some overlying sediment (e.g., Blackman et al., 2022; Daswani et al., 2021). The resolution of geophysical data that are available for Saturn's and Jupiter's moons (spherical harmonic degree/order 2–3) are much too coarse to resolve km-scale seafloor features (e.g., Koh et al., 2022). On that basis, their potential presence cannot be dismissed.

15252027, 2026, 10, Downloaded from https://agupubs.onlinelibrary.wiley.com/doi/10.1029/2026GC012972, Wiley Online Library on [28/10/2026]. See the Terms and Conditions (https://onlinelibrary.wiley.com/terms-and-conditions) on Wiley Online Library for rules of use; OA articles are governed by the applicable Creative Commons License

15252027, 2026, 10, Downloaded from https://agupubs.onlinelibrary.wiley.com/doi/10.1029/2026GC012972, Wiley Online Library on [28/10/2026]. See the Terms and Conditions (https://onlinelibrary.wiley.com/terms-and-conditions) on Wiley Online Library for rules of use; OA articles are governed by the applicable Creative Commons License

Inferences about the density of the rocky interior of Europa and Enceladus and models of their thermal evolution indicate that their shallow subseafloors may be porous (e.g., Roberts, 2015; Travis et al., 2012). The silicate interiors of these moons may not experience present day volcanism or plate tectonics, but past episodes of magmatic activity may have occurred on Europa during periods of strong tidal forcing (Běhounková et al., 2021). Tidal stresses on the rocky interior of these ocean moons are not only a source of dissipative heating (e.g., Tobie et al., 2025), they could generate seafloor displacements of meter scale (e.g., Rambaux et al., 2010), potentially resulting in seafloor fracturing if strain becomes localized. Estimates show that the amount of sediment to have accumulated on the seafloor over their few Gyr history could be up to 100's of m, if sourced from meteorite deposits that are cycled through the ice shell (Blackman et al., 2022), or a kilometer or more, if precipitation from the ocean is the source (Daswani et al., 2021). Furthermore, the action of ocean currents (Soderlund et al., 2024) could lead to uneven sediment deposition or re-distribution on the seafloor. Therefore, it is reasonable to consider the possibility that heterogeneity across the seafloors of other ocean worlds could exist that might focus seawater recharge into, and discharge from, their rocky interiors. Simulations considered in the present study employ km-scale topography, but really the key variability is in seafloor and subseafloor properties (especially permeability).

The scale of the subseafloor temperature variation in the higher permeability Europa simulation (Eu-1, Table 1) is similar to that for the Ea-2 case (±20°C–30°C, Figure S2, Table S1 in Supporting Information S1). This simulation with aquifer permeability 10^{-12} m^2 has 69% of the temperature field within the cylindrical region in the 40°C–80°C range, 29% in the 80°C–120°C range, and 2% less than 40°C. Fluid parcel tracking shows that flow rates in Eu-1 are generally a factor of 3–5 times slower than those in Ea-2. T_f oscillations are commonly ±5°C–10°C but can reach ±20°C. In contrast, when aquifer permeability is an order of magnitude lower (Eu-2), convective cells do not develop and the temperature monotonically increases with depth throughout the aquifer (Figure S2 in Supporting Information S1). Because buoyancy forces scale with gravity, only Europa simulations with higher permeability can overcome resistive intergranular forces to allow local convection to occur (Dickerson et al., 2025; Fisher et al., 2024). While the Europa simulations analyzed here have high basal heat flow (e.g., Běhounková et al., 2021), Dickerson et al. (2025) find that convective cells can develop within a thicker subseafloor aquifer of permeability of 10^{-13} m^2 (or greater), even with very low basal heat flow (10 mW/m^2) and low gravity. Thus, the potential for subseafloor variation in thermal regimes exists if interconnected aquifers occur on other ocean worlds.

The geochemical results from the present study have implications for characterization of potentially habitable environments on other ocean worlds. The organic compounds considered in our examples possess structures consistent with mass fragments detected in icy plume materials expelled from the ocean of Enceladus–amines, alcohols, and benzyl structures (Khawaja et al., 2019; Peter et al., 2024; Postberg et al., 2018a, 2018b). The calculated changes in concentrations of organic compounds in the benzylamine-benzyl alcohol-ammonia system (Section 3.2) provide initial indication that a detectable hydrothermal signature could indeed accrue in fluids that experience the range of subseafloor temperature variability and flow rates that the high end of moderate-T hydrothermal circulation simulations predict (Fisher et al., 2024). Application of this tracer model to a partial flowpath from simulation Eu-1confirms that a signature of hydrothermal activity (>25°C) would be produced relative to a near-freezing ocean, but the average T along the fluid path (75°C–80°C) is too low for the tracers to record it if transit times are less than ∼2 Myr. This general framework, and the likelihood that it may allow application of additional tracer systems such as ethanol-ethene (Robinson et al., 2023) and perhaps others that operate at lower temperatures, point to the importance of measuring suites of organic tracers that could, together, aid in constraining subseafloor conditions that are difficult to measure directly, whether on Earth or other ocean worlds. These findings move beyond previous work that inferred geochemical conditions of Enceladus' ocean based on chemical species that were assumed to instantly equilibrate even at low temperatures (Glein & Waite, 2020). The chemical species discussed here may serve as more informative tracers, even at the icy exteriors of other ocean worlds, when subseafloor hydrothermal systems surpass moderate temperatures (∼80°C), as inferred by Hsu et al. (2015).

4.4. Limitations and Aspects for Further Investigation

The scenarios explored in this study are based on numerous simplifying assumptions, and therefore should be considered to provide a comparative analysis of contrasting conditions rather than specific predictions. For example, aquifer properties were simulated as homogeneous distributions within distinct units, omitting lateral

15252027, 2026, 10, Downloaded from https://agupubs.onlinelibrary.wiley.com/doi/10.1029/2026GC012972, Wiley Online Library on [28/10/2026]. See the Terms and Conditions (https://onlinelibrary.wiley.com/terms-and-conditions) on Wiley Online Library for rules of use; OA articles are governed by the applicable Creative Commons License

variations, barriers to flow, and faults and fractures that are likely to be encountered within ridge flanks below Earth's seafloor (Alt, 2004; Carlson, 2014). Strong tidal forcing could generate/sustain fractures in the outermost rocky interior of the ocean moons of Saturn and Jupiter (e.g., Travis et al., 2012) and this could result in heterogeneously distributed permeability at the seafloor. Regardless of the mechanism, if the scale/magnitude of permeability variation is sufficient to alter the flow pattern, then the occurrence and nature of convective cells will be impacted. There is a reasonable likelihood for scenarios to exist where the aquifer layer is thin relative to the distance between recharge and discharge sites, particularly at permeabilities that are common for crystalline rocks subjected to modest effective stresses. Patterns of fluid convection are likely to be influenced by variability in formation properties, including circulation depth and the lateral extent of connectivity. This study focused on rolling convection within a subseafloor hydrothermal aquifer having relatively uniform properties-more heterogeneous systems should experience even more variability in thermal and chemical conditions.

Basal heat flow in most of the simulations presented was 196 mW/m^2, which is appropriate for relatively young ocean crust on Earth, but is higher than both Earth's global mean and that predicted to reach the seafloor of many other ocean worlds (Choblet et al., 2017; Davies & Davis, 2010; Hussman et al., 2002). A study of Earth's seafloor has shown that having a hydrogeologic restriction at the discharge end of a hydrothermal circulation path ("discharge domination" as defined by Cann & Strens, 1989) can help to retain elevated temperatures below the seafloor. In general, lower heat input at depth tends to reduce temperatures and flow rates, but relatively higher subseafloor temperatures can be attained if discharge restrictions occur at the seafloor. In addition, elevated temperatures, including the ranges explored in this study, can be achieved even if basal heat flow is much lower, provided fluids are permitted to circulate to somewhat greater depths within the rocky interior. In all of these cases, except for the lowest values of gravity and heat input, associated buoyancy forces can drive small-scale convection and corresponding subseafloor temperature variability.

Additional studies are underway to extend this work and examine the potential influence of heterogeneous properties in the rocky interior of an ocean world, using porous and discrete-fractured media physics to define aquifer properties (Dickerson et al., 2025). Those studies include low basal heat flow (10 mW/m^2), Europa's low gravity, and a rocky aquifer up to 10 km thick. Preliminary results show that local convection cells develop in some of those simulations, with persistent T variability predicted to be greatest for a homogeneous permeable matrix aquifer. Scenarios including a discrete fracture network assumed a power-law distribution of fault lengths ranging 1–10 km, randomly distributed and oriented, throughout the aquifer. For cases with fracture permeability throughout the network set at 1-2 orders of magnitude greater than the surrounding matrix, km-scale lateral variation in aquifer temperatures was reduced compared to the matrix-only case, but not eliminated (Dickerson et al., 2025). This suggests that our simulations with homogeneous effective permeability can provide a useful bound on subseafloor temperature variability.

We did not address the effects of reactive transport in this study. We acknowledge that dissolution and remineralization often occur at different locations along fluid pathways in oceanic basements (e.g., Alt, 2004). Here, we focus on a baseline scenario to illuminate the scale of variability that could occur in the physical system alone. This is an important starting point that illustrates conceptually the potential importance of corresponding subseafloor geochemical and microbial variability. Reactive transport models require many more assumptions than our basic, linked physical and geochemical calculations. Many of the necessary prescribed parameters for reactive transport are poorly known for Earth's subseafloor hydrothermal systems and are almost unknown for other ocean worlds. In this situation, the ability to fairly quickly estimate the scale of influence that certain parameters have on envisioned scenarios can be key to gaining fundamental insights. Such new understanding can serve as a guide for designing more computationally intensive future simulations that incorporate chemical exchange as well as complex fluid flow.

Finally, our findings on the scale of subseafloor temperature variability and its rates of change, both in the formation water that is discharged back to the ocean and for fluid parcels circulating beneath the seafloor, provide strong motivation for future coupled flow/T modeling efforts to include explicit particle tracking. Our current 'snapshot' results cannot capture the actual temporal evolution of fluids along an aquifer, which could form a basis for testing specific predictions for well-studied (Earth) seafloor systems. For much of the time, convection cells in the models roll steadily along the aquifer, as approximated with synoptic output. However, for some models, there are times when the system becomes unstable and rapid flow reconfiguration occurs (Fisher et al., 2024; Winslow et al., 2016). Only by explicitly tracking particles throughout a simulation will it be possible to assess the

15252027, 2026, 10, Downloaded from https://agupubs.onlinelibrary.wiley.com/doi/10.1029/2026GC012972, Wiley Online Library on [28/10/2026]. See the Terms and Conditions (https://onlinelibrary.wiley.com/terms-and-conditions) on Wiley Online Library for rules of use; OA articles are governed by the applicable Creative Commons License

temperature changes, and associated geochemical/biological implications, of such events. This study underscores how the extra computational effort needed to track particles, and associated thermal and chemical conditions, can be justified.

5. Summary and Conclusions

This study obtained an initial assessment of the scale of subseafloor temperature variability that could arise within the shallow aquifer of a thermally-driven hydrothermal system where discharged fluids exhibit modest temperatures (70°C–110°C). The results provide a new understanding of the temporal and spatial scales of variability that could occur when recharge and discharge sites are separated by 10s of kilometers. The models explored here are underpinned by numerical simulations that predict discharge flow rates and surrounding heat flow that match observations for a seamount-to-seamount siphon on the 3.5 Ma eastern flank of the Juan de Fuca ridge. Rather than making specific predictions for this system, our findings shed light on subseafloor variability that might generally characterize low-flow systems where the aquifer is very thin, relative to the distance between recharge and discharge sites, and has permeability in the 10^{-12}–10^{-13} range; it is plausible that this same approach could apply for ocean worlds beyond Earth. For a scenario where the effective permeability of the aquifer is homogeneous, we find that: (a) the temperature of the rock could vary by ±10°C–30°C over lateral distances of the order of a kilometer; (b) the rates of temperature change in basement rock could be of the order 0.2–3.0°C/1,000 yr, and (c) the rates of temperature change for fluid parcels circulating through the aquifer could reach 10°C/1000 yr. These scales of subseafloor variability and rates of change have implications for the diversity of geochemical reaction rates and alteration mineralogy that may result, as well as the possible distribution/viability of microbial ecosystems that could be sustained within such subseafloor environments.

Conflict of Interest

The authors declare no conflicts of interest relevant to this study.

Availability Statement

The computer simulation code and results that underpin the temperature variability investigation were made available in a previous publication (Fisher et al., 2024). The geochemical data and methods were also previously made available in Randolph-Flagg et al. (2023), Robinson et al. (2021b), and Winslow and Fisher (2015).

Acknowledgments
This work was supported by NASA Astrobiology Grant 80NSSC19K1427 and ICAR award 80NSSC26K0263. The concept arose from discussions with Chris German and Jeff Seewald while Donna Blackman was visiting WHOI with support from the Keck Graduate Seminar fund. General discussions with the full Exploring Ocean Worlds project team provided important context.

References

Akiba, R., & Fisher, A. T. (2025). Parameter space exploration of low-to-moderate temperature hydrothermal systems on ocean worlds using a Monte Carlo framework. *The Planetary Science Journal*, *6*(9), 210. https://doi.org/10.3847/PSJ/adf558

Alt, J. A. (2004). Alteration of upper oceanic crust: Mineralogy, chemistry and processes. In E. Davis & H. Elderfield (Eds.), *Hydrogeology of the oceanic lithosphere E* (pp. 456–488). Cambridge University Press.

Amend, J. P. T. M. M. C., Hentscher, M., & Bach, W. (2011). Catabolic and anabolic energy for chemotlithoautotrophs in deep-sea hydrothermal systems hosted in different rock types. *Geochimica et Cosmochimica Acta*, *75*. https://doi.org/10.1016/j.gca.2011.07.041

Anderson, B. W., Coogan, L. A., & Gillis, K. M. (2012). The role of outcrop-to-outcrop fluid flow in off-axis oceanic hydrothermal systems under abyssal sedimentation conditions. *Journal of Geophysical Research*, *117*(B5), B05103. https://doi.org/10.1029/2011JB009052

Anderson, R. N., Zoback, M. D., Hickman, S. H., & Newmark, R. L. (1985). Permeability versus depth in the upper oceanic crust: In situ measurements in DSDP hole 504B, eastern equatorial Pacific. *Journal of Geophysical Research: Solid Earth*, *90*(B5), 3659–3669. https://doi.org/10.1029/JB090iB05p03659

Bach, W. (2016). Some compositional and kinetic controls on the bioenergetic landscapes in Oceanic basement. *Frontiers in Microbiology*, *7*. https://doi.org/10.3389/fmicb.2016.00107

Baker, P. A., Stout, P. M., Kastner, M., & Elderfield, H. (1991). Large-scale lateral advection of seawater through oceanic crust in the central equatorial Pacific. *Earth and Planetary Science Letters*, *105*(4), 522–533. https://doi.org/10.1016/0012-821x(91)90189-o

Běhounková, M., Tobie, G., Choblet, G., Kervazo, M., Melwani Daswani, M., Dumoulin, C., & Vance, S. D. (2021). Tidally induced magmatic pulses on the oceanic floor of Jupiter's moon Europa. *Geophysical Research Letters*, *48*(3), e2020GL090077. https://doi.org/10.1029/2020GL090077

Blackman, D. K., Randolph-Flagg, N., Fisher, A. T., Price, A. N., Mittal, T., & Sotin, C. (2022) Seafloor variability on Ocean Worlds- potential influences of relief and meteoritic sedimentation on hydrothermal flow pattern. In *AbSciCon 2022*. Abstract 247-02. Retrieved from https://studio.m-anage.com/agu/abscicon21/meetingapp.cgi/Paper/1026628

Boyer, G. (2024). pyCHNOSZ: Python wrapper for the thermodynamic package CHNOSZ (v0.8.15). *Zenodo*. https://doi.org/10.5281/zenodo.11406142

Cadek, O., Kalousova, K., Kvorka, J., & Sotin, C. (2021). The density structure of Titan's outer ice shell. *Icarus*, *364*, 114466. https://doi.org/10.1016/j.icarus.2021.114466

Cann, J., & Strens, M. R. (1989). Modeling periodic megaplume emission by blavk smoker systems. *Journal of Geophysical Research*, *94*(B9), 12227–12237. https://doi.org/10.1029/JB094iB09p12227

Carbotte, S. M., Canales, J.-P., Nedimovic, M. R., Carton, H., & Mutter, J. C. (2012). Recent seismic studies at the East Pacific rise 8°20′–10°10′N and Endeavour segment: Insights into mid-ocean ridge hydrothermal and magmatic processes. *Oceanography*, *25*(1), 100–112. https://doi.org/10.5670/oceanog.2012.08

Carlson, R. L. (2014). The effects of alteration and porosity on seismic velocities in oceanic basalts and diabases. *Geochemistry, Geophysics, Geosystems*, *15*(12), 4589–4598. https://doi.org/10.1002/2014GC005537

Choblet, G., Tobie, G., Sotin, C., Behounkova, M., Cadek, O., Postberg, F., & Soucek, O. (2017). Powering prolonged hydrothermal activity inside Enceladus. *Nature Astronomy*, *1*(12), 841–847. https://doi.org/10.1038/s41550-017-0289-8

Clague, D. A., Martin, J. F., Paduan, J. B., Butterfield, D. A., Jamieson, J. W., Le Saut, M., et al. (2020). Hydrothermal chimney distribution on the Endeavour segment, Juan de Fuca ridge. *Geochemistry, Geophysics, Geosystems*, *21*(6), e2020GC008917. https://doi.org/10.1029/2020GC008917

Coggon, R. M., Evans, A. D., Grant, L. J. C., & Teagle, D. A. H. (2025). Low-Temperature ridge flank heat and fluid fluxes, contributions to global biogeochemical cycles, and archives of changing global conditions. In *Hydrothermal circulation and seawater chemistry* (pp. 187–224). https://doi.org/10.1002/9781394229185

Coogan, L. A., & Gillis, K. M. (2018a). Low-temperature alteration of the seafloor: Impacts on ocean chemistry. *Annual Review of Earth and Planetary Sciences*, *46*(1), 21–45. https://doi.org/10.1146/annurev-earth-082517-010027

Coogan, L. A., & Gillis, K. M. (2018b). Temperature dependence of chemical exchange during seafloor weathering: Insights from the Troodos ophiolite. *Geochimica et Cosmochimica Acta*, *243*, 24–41. https://doi.org/10.1016/j.gca.2018.09.025

Cruse, A. M., & Seewald, J. S. (2006). Geochemistry of low-molecular weight hydrocarbons in hydrothermal fluids from Middle Valley, northern Juan de Fuca Ridge. *Geochimica et Cosmochimica Acta*, *70*(8), 2073–2092. https://doi.org/10.1016/j.gca.2006.01.015

Daswani, M., Vance, S. D., Mayne, M. J., & Glein, C. R. (2021). A metamorphic origin for Europa's Ocean. *Geophysical Research Letters*, *48*. https://doi.org/10.1029/2021GL094143

Davies, J. H., & Davis, D. R. (2010). Earth's surface heat flux. *Solid Earth*, *1*, 5–24. https://doi.org/10.5194/se-1-5-2010

Davis, E. E., Chapman, D. S., Mottl, M. J., Bentkowski, W. J., Dadey, K., Forster, C., et al. (1992). FlankFlux: An experiment to study the nature of hydrothermal circulation in young oceanic crust. *Canadian Journal of Earth Sciences*, *29*(5), 925–952. https://doi.org/10.1139/e92-078

Davis, E. E., Wang, K., Becker, K., & Thompson, R. E. (2000). Formation-scale hydraulic and mechanical properties of oceanic crust inferred from pore-pressure response to periodic seafloor loading. *Journal of Geophysical Research*, *105*(B6), 13423–13435. https://doi.org/10.1029/2000jb900084

Delaney, J. R., Kelley, D., Lilley, M., Butterfield, D., Mcduff, R., Baross, J., et al. (1997). The Endeavour hydrothermal system I: Cellular circulation above an active cracking front yields large sulfide structures, "fresh" vent water, and hyperthermophilic archaea, RIDGE events, *8*, 11–19.

de Martin, B. J., Sohn, R. A., Canales, J.-P., & Humphris, S. E. (2007). Kinematics and geometry of active detachment faulting beneath the TAG hydrothermal field on the Mid-atlantic ridge. *Geology*, *35*. https://doi.org/10.11230/G23718A.1

Dick, J. M. (2019). CHNOSZ: Thermodynamic calculations and diagrams for geochemistry. *Frontiers in Earth Science*, *7*, 180. https://doi.org/10.3389/feart.2019.00180

Dickerson, K. L., Fisher, A. T., Hyman, J., Stauffer, P., Ortiz, J. P., & Blackman, D. K. (2025). Potential for porous and discrete-fracture hydrothermal circulation below the seafloor of Europa, given low gravity and modest internal heating. In *AGU Fall Meeting Abstracts* (2717), (p. P23E-2717).

Dunn, R. A., & Forsyth, D. W. (2003). Imaging the transition between the region of mantle melt generation and the crustal magma chamber beneath the southern East Pacific rise with short-period love waves. *Journal of Geophysical Research*, *108*(B7). https://doi.org/10.1029/2002JB002217

Elderfield, H., & Schultz, A. (1996). Mid-ocean ridge hydrothermal fluxes and the chemical composition of the ocean. *Annual Review of Earth and Planetary Sciences*, *24*(1), 191–224. https://doi.org/10.1146/annurev.earth.24.1.191

Elderfield, H., Wheat, C. G., Mottl, M. J., Monnin, C., & Spiro, B. (1999). Fluid and geochemical transport through oceanic crust: A transect across the eastern flank of the Juan de Fuca Ridge. *Earth and Planetary Science Letters*, *172*(1–2), 151–165. https://doi.org/10.1016/S0012-821X(99)00191-0

Ely, T. D., Leong, J. M., Canovas, P. A., & Shock, E. L. (2023). Huge variation in H2 generation during seawater alteration of ultramafic rocks. *Geochemistry, Geophysics, Geosystems*, *24*(3), e2022GC010658. https://doi.org/10.1029/2022GC010658

Fisher, A. T., Alt, J. C., & Bach, W. (2014). Hydrogeologic properties, processes and alteration in the igneous ocean crust. In R. Stein, D. Blackman, F. Inagaki, & H.-C. Larsen (Eds.), *Earth and life processes discovered from subseafloor environment—A decade of science achieved by the integrated ocean drilling program (IODP)* (pp. 507–551). Elsevier. https://doi.org/10.1016/B978-0-444-62617-2.00018-9

Fisher, A. T., & Becker, K. (2000). Channelized fluid flow in oceanic crust reconciles heat-flow and permeability data. *Nature*, *403*(6765), 71–74. https://doi.org/10.1038/47463

Fisher, A. T., Davis, E. E., Hutnak, M., Spiess, V., Zuhlsdorff, L., Cherkaoui, A., et al. (2003). Hydrothermal circulation across 50 km on a young ridge flank: The role of seamounts in guiding recharge and discharge at a crustal scale. *Nature*, *421*. https://doi.org/10.1038/nature01352

Fisher, A. T., Dickerson, K. L., Blackman, D. K., Randolph-Flagg, N. G., German, C., & Sotin, C. (2024). Sustaining hydrothermal circulation with gravity relevant to ocean worlds. *Journal of Geophysical Research: Planets*, *129*, e2023JE008202. https://doi.org/10.1029/2023je008202

Fisher, A. T., & Harris, R. N. (2010). Using seafloor heat flow as a tracer to map subseafloor fluid flow in the ocean crust. *Geofluids*, *10*(1–2), 142–160. https://doi.org/10.1111/j.1468-8123.2009.00274.x

Fisher, A. T., & Wheat, C. G. (2010). Seamounts as conduits for massive fluid, heat, and solute fluxes on ridge flanks. *Oceangraphy*, *23*(1), 74–87. https://doi.org/10.5670/oceanog.2010.63

Fortunato, C. S., Larson, B., Butterfield, D. A., & Huber, J. A. (2018). Spatially distinct, temporally stable microbial populations mediate biogeochemical cycling at and below the seafloor in hydrothermal vent fluids. *Environmental Microbiology*, *20*(2), 769–784. https://doi.org/10.1111/1462-2920.14011

German, C. R., Lang, S. Q., & Fitzsimmons, J. N. (2025). Marine hydrothermal processes. *Treat. Geochemistry*, *4*, 145–176. https://doi.org/10.1016/B978-0-323-99762-1.00048-6

Glein, C. R., & Waite, J. H. (2020). The carbonate geochemistry of Enceladus' ocean. *Geophysical Research Letters*, *47*(3), e2019GL085885. https://doi.org/10.1029/2019GL085885

Haitjema, H. M. (1995). *Analytic element modeling of groundwater flow*. Academic Press. https://doi.org/10.1016/B978-0-12-316550-3.X5000-4

Hand, K. P., & German, C. R. (2018). Exploring ocean worlds on Earth and beyond. *Nature Geoscience*, *11*(1), 2–4. https://doi.org/10.1038/s41561-017-0045-9

Hasterok, D. (2013). Global patterns and vigor of ventilated hydrothermal circulation through young seafloor. *Earth and Planetary Science Letters*, *380*, 12–20. https://doi.org/10.1016/j.epsl.2013.08.016

15252027, 2026, 10, Downloaded from https://agupubs.onlinelibrary.wiley.com/doi/10.1029/2026GC012972, Wiley Online Library on [28/10/2026]. See the Terms and Conditions (https://onlinelibrary.wiley.com/terms-and-conditions) on Wiley Online Library for rules of use; OA articles are governed by the applicable Creative Commons License

Haymon, R. M., Fornari, D. J., Edwards, M. H., Carbotte, S., Wright, D., & Macdonald, K. C. (1991). Hydrothermal vent distribution along the East Pacific Rise crest (9°09'-54'N) and its relationship to magmatic and tectonic processes on fast-spreading mid-ocean ridges. *Earth and Planetary Science Letters*, *104*(2–4), 513–534. https://doi.org/10.1016/0012-821X(91)90226-8

Helgeson, H. C., Knox, A. M., Owens, C. E., & Shock, E. L. (1993). Petroleum, oil field waters, and authigenic mineral assemblages are they in metastable equilibrium in hydrocarbon reservoirs. *Geochimica et Cosmochimica Acta*, *57*(14), 3295–3339. https://doi.org/10.1016/0016-7037(93)90541-4

Hemingway, D. J., & Mittal, T. (2019). Enceladus's ice shell structure as a window on internal heat production. *Icarus*, *332*, 111–131. https://doi.org/10.1016/j.icarus.2019.03.011

Hoehler, T. M. (2004). Biological energy requirements as quantitative boundary conditions for life in the subsurface. *Geobiology*, *2*(4), 205–215. https://doi.org/10.1111/j.1472-4677.2004.00033.x

Hsu, H.-W., Postberg, F., Sekine, Y., Shibuya, T., Kempf, S., Horányi, M., et al. (2015). Ongoing hydrothermal activities within Enceladus. *Nature*, *519*(7542), 207–210. https://doi.org/10.1038/nature14262

Huber, J. A., & Holden, J. F. (2008). Modeling the impact of diffuse vent microorganisms along mid-ocean ridges and flanks. *Magma to Microbe: Modeling hydrothermal processes at ocean spreading centers*, *178*, 215–231. https://doi.org/10.1029/GM178

Humphris, S. E., Zierenberg, R. A., Mullineaux, L. S., & Thomson, R. E. (1995). Seafloor hydrothermal systems. In *Geophysical Monograph Series* (Vol. 91).

Hussman, H., Spohn, T., & Wieczerkowski, K. (2002). Thermal equilibrium states of Europa's Ice shell: Implications for Internal ocean thickness and surace heat flow. *Icarus*, *156*. https://doi.org/10.1006/icar.2001.6776

Hutnak, M., Fisher, A. T., Harris, R., Stein, C., Wang, K., Spinelli, G., et al. (2008). Large heat and fluid fluxes driven through mid-plate outcrops on ocean crust. *Nature Geoscience*, *1*(9), 611–614. https://doi.org/10.1038/ngeo264

Hutnak, M., Fisher, A. T., Zuhlsdorff, L., Spiess, V., Stauffer, P. H., & Gable, C. W. (2006). Hydrothermal recharge and discharge guided by basement outcrops on 0.7–3.6 Ma seafloor east of the Juan de Fuca ridge: Observations and numerical models. *Geochemistry, Geophysics, Geosystems*, *7*. https://doi.org/10.1029/2006GC001242

Jannasch, H. W., & Mottl, M. J. (1985). Geomicrobiology of deep-sea hydrothermal vents. *Science*, *229*(4715), 717–725. https://doi.org/10.1126/science.229.4715.717

Johnson, H. P., & Pruis, M. J. (2003). Fluxes of fluid and heat from the oceanic crustal reservoir. *Earth and Planetary Science Letters*, *216*(4), 565–574. https://doi.org/10.1016/S0012-821X(03)00545-4

typo- should be Jungbluth

Junbluth, S. P. R. M. B., Lin, H. 0T., Cowen, J. P., & Rappe, M. S. (2016). Novel microbial assemblages inhaginting crustal fluids within mid-0ocean ridge flank subsurface basalt. *J. Microb. Ecology*, *10*. https://doi.org/10.1038/ismej.2015.248

Khawaja, N., Postberg, F., Hillier, J., Klenner, F., Kempf, S., Nölle, L., et al. (2019). Low-mass nitrogen-oxygen-bearing, and aromatic compounds in Enceladean ice grains. *Monthly Notices of the Royal Astronomical Society*, *489*(4), 5231–5243. https://doi.org/10.1093/mnras/stz2280

Koh, Z.-W., Nimmo, F., Lunine, J. L., Mazarico, E., & Dombard, A. J. (2022). Assessing the detectability of Europa's seafloor topography from Europa Clipper's gravity data, Planet. *Sci-journal*, *3*(8), 197. https://doi.org/10.3847/PSJ/ac82aa

Kremin, I., Guo, Z., & Rüpke, L. (2024). Evaluating the physics of outcrop-to-outcrop flow with hydrothermal fow models. *Geochemistry, Geophysics, Geosystems*, *25*(7), e2024GC011529. https://doi.org/10.1029/2024GC011529

Langseth, M. G., & Herman, B. (1981). Heat transfer in the oceanic crust of the Brazil Basin. *Journal of Geophysical Research*, *86*(B11), 10805–10819. https://doi.org/10.1029/jb086ib11p10805

Lauer, R. M., Fisher, A. T., & Winslow, D. M. (2018). Three-dimensional models of hydrothermal circulation through a semount network on fast-spreading cruse. *Earth and Planetary Science Letters*, *501*. https://doi.org/10.1016/j.icarus.2021.114466

Lee, W., Chen, M. A., Bresciani, E., Toner, B. M., & Kang, P. K. (2025). Effects of pore-scale three-dimensional flow and fluid inertia on mineral dissolution. *Water Resources Research*, *61*, e2024WR038176. https://doi.org/10.1029/2024WR038176

Le Gal, V., Lucazeau, F., Cannat, M., Poort, J., Monnin, C., Battani, A., et al. (2018). Heat flow, morphology, pore fluids and hydrothermal circulation in a typical mid-atlantic ridge flank near oceanographer fracture zone. *Earth and Planetary Science Letters*, *482*, 423–433. https://doi.org/10.1016/j.epsl.2017.11.035

Lever, M. A., Rouxel, O., Alt, J. C., Shimizu, N., Ono, S., Coggon, R. M., et al. (2013). Evidence for microbial carbon and sulfur cycling in deeply buried ridge flank basalt. *Science*, *339*(6125), 1305–1308. https://doi.org/10.1126/science.1229240

Malamud, U., & Prialnik, D. (2013). Modeling serpentization: Applied to the early evolution of enceladus and Mimas. *Icarus*, *225*(1), 763–774. https://doi.org/10.1016/j.icarus.2013.04.024

McDermott, J. M., Seewald, J. S., German, C. R., & Sylva, S. P. (2015). Pathways for abiotic organic synthesis at submarine hydrothermal fields. *Proceedings of the National Academy of Sciences*, *112*(25), 7668–7672. https://doi.org/10.1073/pnas.1506295112

McKinnon, W. B. (2013). The shape of Enceladus as explained by an irregular core: Implications for gravity, librations, and survival of its subsurface ocean. *Journal of Geophysical Research*, *118*(9), 1775–1788. https://doi.org/10.1002/jgre.20122

Miller, N. C., Lizarralde, D., Collins, J. A., Holbrook, W. S., & van Avendonk, H. J. A. (2020). Limited mantle hydration by bending faults at the Middle America trench. *Journal of Geophysical Research*, *126*(1), e2020JB020982. https://doi.org/10.1029/2020JB020982

Mottl, M. (2003). Oceanic phosporous imbalance: Magnitude of the mid-ocean ridge flank hydrothermal sink. *Geophysical Research Letters*, *30*. https://doi.org/10.1029/2003GL017318

Mottl, M. J., Wheat, C. G., Baker, E., Becker, N., Davis, E., Feeley, R., et al. (1998). Warm springs discovered on 3.5 Ma oceanic crust, eastern flank of the Juan de Fuca Ridge. *Geology*, *26*(1), 51–54. https://doi.org/10.1130/0091-7613(1998)026<0051:WSDOMO>2.3.CO;2

Moulana, A., Anderson, R., Fortunato, C., & Huber, J. (2020). Selection is a significant driver of gene gain and loss in the pangenome of the bacterial genus Sulfurovum in geographically distinct deep-sea hydrothermal vents. *mSystems*, *20*(2), e00673-19. https://doi.org/10.1128/msystems.00673-19

Neira, N. M., Clark, J. F., Fisher, A. T., Wheat, C. G., Haymon, R. M., & Becker, K. (2016). Cross-hole tracer experiment reveals rapid fluid flow and low effective porosity in the upper oceanic crust. *Earth and Planetary Science Letters*, *450*, 355–365. https://doi.org/10.1016/j.epsl.2016.06.048

Nimmo, F., & Pappalardo, R. T. (2016). Ocean worlds in the outer solar system. *Journal of Geophysical Research: Planets*, *121*(8), 1378–1399. https://doi.org/10.1002/2016JE005081

Norvell, B., Kyritz, T., Spinelli, G. A., Harris, R. N., Dickerson, K., Tréhu, A. M., et al. (2023). Thermally significant fluid seepage through thick sediment on the Juan de Fuca plate entering the Cascadia subduction zone. *Geochemistry, Geophysics, Geosystems*, *24*(8), e2023GC010868. https://doi.org/10.1029/2023GC010868

Peter, J. S., Nordheim, T. A., & Hand, K. P. (2024). Detection of HCN and diverse redox chemistry in the plume of Enceladus. *Nature Astronomy*, *8*(2), 164–173. https://doi.org/10.1038/s41550-023-02160-0

15252027, 2026, 10, Downloaded from https://agupubs.onlinelibrary.wiley.com/doi/10.1029/2026GC012972, Wiley Online Library on [28/10/2026]. See the Terms and Conditions (https://onlinelibrary.wiley.com/terms-and-conditions) on Wiley Online Library for rules of use; OA articles are governed by the applicable Creative Commons License

Pollock, D. W. (2016). *User guide for MODPATH version 7 -- A particle-tracking model for MODFLOW* (p. 35). U.S. Geological Survey Open-File Report 2016-1086. https://doi.org/10.3133/ofr20161086

Postberg, F., Clark, R. N., Hansen, C. J., Coates, A. J., Ore, C. M. D., Scipioni, F., et al. (2018a). Plume and surface composition of Enceladus. In P. M. Schenk, R. N. Clark, C. J. A. Howett, A. J. Verbiscer, & J. H. Waite (Eds.), *Enceladus and the icy moons of Saturn* (pp. 129–162). University of Arizona Press. https://doi.org/10.2458/azu_uapress_9780816537075-ch007

Postberg, F., Khawaja, N., Abel, B., Choblet, G., Glein, C. R., Gudipati, M. S., et al. (2018b). Macromolecular organic compounds from the depths of Enceladus. *Nature*, *558*(7711), 564–568. https://doi.org/10.1038/s41586-018-0246-4

Price, A. N., Fisher, A. T., Stauffer, P. H., & Gable, C. W. (2021). Numerical simulation of cool hydrothermal processes in the upper volcanic crust beneath a marine sediment pond: North Pond, North Atlantic Ocean. *Journal of Geophysical Research*, *127*(1), e2021JB023158. https://doi.org/10.1029/2021JB023158

Rambaux, N., Castillo-Rogez, J. C., Williams, J. G., & Karatekin, Ö. (2010). Librational response of Enceladus. *Geophysical Research Letters*, *37*(4), L04202. https://doi.org/10.1029/2009GL041465

Randolph-Flagg, N. G., Ely, T., Som, S., Shock, E., German, C., & Hoehler, T. (2023). Phosphorus availability and implications for life on ocean worlds. *Nature Communications*, *14*(1), 2388. https://doi.org/10.1038/s41467-023-37770-9

Reveillaud, J., Reddington, E., McDermott, J., Algar, C., Meyer, J. L., Sylva, S., et al. (2015). Subseafloor microbial communities in hydrogen-rich vent fluids from hydrothermal systems along the Mid-Cayman Rise. *Environmental Microbiology*, *18*(6), 1970–1987. https://doi.org/10.1111/1462-2920.13173

Robador, A., Jungbluth, S. P., LaRowe, D. E., Bowers, R. M., Rappé, M. S., Amend, J. P., & Cowen, J. P. (2015). Activity and phylogenetic diversity of sulfate-reducing microorganisms in low-temperature subsurface fluids within the upper oceanic crust. *Frontiers in Microbiology*, *5*. https://doi.org/10.3389/fmicb.2014.00748

Roberts, J. H. (2015). The fluffy core of Enceladus. *Icarus*, *258*, 54–66. https://doi.org/10.1016/j.icarus.2015.05.033

Robinson, K. J., Bockisch, C., Gould, I. R., Liao, Y., Yang, Z., Glein, C. R., et al. (2021a). Quantifying the extent of amide and peptide bond synthesis across conditions relevant to geologic and planetary environments. *Geochim.Cosmo. Acta*, *300*, 318–332. https://doi.org/10.1016/j.gca.2021.01.038

Robinson, K. J., Fecteau, K. M., Gould, I. R., Hartnett, H. E., Williams, L. B., & Shock, E. L. (2020). Metastable equilibrium of substitution reactions among oxygen-and nitrogen-bearing organic compounds at hydrothermal conditions. *Geochimica et Cosmochimica Acta*, *272*, 93–104. https://doi.org/10.1016/j.gca.2019.12.030

Robinson, K. J., Gould, I. R., Hartnett, H. E., Williams, L. B., & Shock, E. L. (2021b). Hydrothermal experiments with protonated benzylamines provide predictions of temperature-dependent deamination rates for geochemical modeling. *ACS Earth and Space Chemistry*, *5*(8), 1997–2012. https://doi.org/10.1021/acsearthspacechem.1c00104

Robinson, K. J., Hartnett, H. E., Gould, I. R., & Shock, E. L. (2023). Ethene-ethanol ratios as potential indicators of hydrothermal activity at Enceladus, Europa, and other icy ocean worlds. *Icarus*, *406*, 115765. https://doi.org/10.1016/j.icarus.2023.115765

Robinson, K. J., Seewald, J. S., Sylva, S. P., Fecteau, K. M., & Shock, E. L. (2024). Thermodynamic property estimations for aqueous primary, secondary, and tertiary alkylamines, benzylamines, and their corresponding aminiums across temperature and pressure are validated by measurements from experiments. *Geochimica et Cosmochimica Acta*, *372*, 62–80. https://doi.org/10.1016/j.gca.2024.03.013

Robinson, K. J., Shock, E. L., Sylva, S. P., & Seewald, J. S. (2026). Hydrothermal experiments reveal methanol, ammonia, and methylamines as tracers of pH and temperature with potential application to Enceladus, Europa, and other icy ocean worlds. *Geochimica et Cosmochimica Acta*. https://doi.org/10.1016/j.gca.2026.09.013

Salaree, A., & Okal, E. A. (2020). Effects of bathymetry complexity on tsunami propagation: A spherical harmonics approach. *Geophysical Journal International*, *223*(1), 632–647. https://doi.org/10.1093/gji/ggaa334

Sandwell, D. T., Smith, W. H. F., Garcia, E., & Francis, R. (2014). New global marine gravity model from CryoSat-2 and Jason-1 reveals buried tectonic structure. *Science*, *346*(6205), 65–67. https://doi.org/10.1126/science.1258213

Schröder, A., & Schanz, D. (2023). 3D lagrangian particle tracking in fluid mechanics. *Annual Review of Fluid Mechanics*, *55*(1), 511–540. https://doi.org/10.1146/annurev-fluid-031822-041721

Schubert, G., Anderson, J. D., Spohn, T., & McKinnon, W. B. (2004). Interior composition, structure, and dynamics of the Galilean satellites. In F. Bagenal, T. E. Dowling, & W. B. McKinnon (Eds.), *Jupiter. The planet, satellites, and magnetosphere* (pp. 281–306). Cambridge University Press.

Seewald, J. S. (1994). Evidence for metastable equilibrium between hydrocarbons under hydrothermal conditions. *Nature*, *370*(6487), 285–287. https://doi.org/10.1038/370285a0

Seewald, J. S. (2001). Aqueous geochemistry of low molecular weight hydrocarbons at elevated temperatures and pressures: Constraints from mineral buffered laboratory experiments. *Geochimica et Cosmochimica Acta*, *65*(10), 1641–1664. https://doi.org/10.1016/S0016-7037(01)00544-0

Seewald, J. S., Wheat, C. G., Reeves, E. P., Tivey, M. K., Sievert, S. M., Stakes, D., et al. (2024). Spatial evolution and temporal stability of hydrothermal processes at sediment-covered spreading centers: Constraints from Guaymas Basin, Gulf of California. *Geochimica et Cosmochimica Acta*, *367*, 87–106. https://doi.org/10.1016/j.gca.2023.12.006

Shock, E. L. (1988). Organic acid metastability in sedimentary basins. *Geology*, *16*(10), 886–890. https://doi.org/10.1130/0091-7613(1988)016<0886:oamisb>2.3.co;2

Shock, E. L. (1989). Corrections to organic acid metastability in sedimentary basins. *Geology*, *17*(6), 572–573. https://doi.org/10.1130/0091-7613(1989)017<0572:ctoami>2.3.co;2

Soderlund, K. M., Rovire-Navarro, M., Le Bars, M., Schmidt, B. E., & Gerkema, T. (2024). The physical oceanography of ice-covered moons. *Annual Review of Marine Science*, *16*. https://doi.org/10.1146/annurev-marine-040323-101355

Spinelli, G. A., Giambalvo, E. R., & Fisher, A. T. (2004). Sediment permeability, distribution, and influence on fluxes in oceanic basement. In E. E. Davis & H. Elderfield (Eds.), *Hydrogeology of the oceanic lithosphere* (p. 151). Cambridge University Press

Stein, J. S., & Fisher, A. T. (2003). Observations and models of lateral hydrothermal circulation on a young ridge flank: Numerical evaluation of thermal and chemical constraints. *Geochemistry, Geophysics, Geosystems*, *4*(3). https://doi.org/10.1029/2002GC000415

Takai, K., Nakamura, K., Toki, T., Tsunogai, U., Miyazaki, M., Miyazaki, J., et al. (2008). Cell proliferation at 122°C and isotopically heavy CH4 production by a hyperthermophilic methanogen under high-pressure cultivation. *Proceedings of the National Academy of Sciences of the United States of America*, *105*(31), 10949–10954. https://doi.org/10.1073/pnas.0712334105

Tassi, F., Vaselli, O., Capaccioni, B., Montegrossi, G., Barahona, F., & Caprai, A. (2007). Scrubbing process and chemical equilibria controlling the composition of light hydrocarbons in natural gas discharges: An example from the geothermal fields of El Salvador. *Geochemistry, Geophysics, Geosystems*, *8*(5). https://doi.org/10.1029/2006GC001487

15252027, 2026, 10, Downloaded from https://agupubs.onlinelibrary.wiley.com/doi/10.1029/2026GC012972, Wiley Online Library on [28/10/2026]. See the Terms and Conditions (https://onlinelibrary.wiley.com/terms-and-conditions) on Wiley Online Library for rules of use; OA articles are governed by the applicable Creative Commons License

Tobie, G., Auclair-Desrotour, P., Behoundova, M., Kervazo, M., Soucek, O., & Kalousova, K. (2025). Tidal deformation and dissipation processes in icy worlds. *Space Science Reviews*, *221*. https://doi.org/10.1007/s11214-025-01136-y

Tolstoy, M., Waldhauser, F., Bohnenstiehl, D. R., Weekly, R. T., & Kim, W.-Y. (2008). Seismic identification of along-axis hydrothermal flow on the East Pacific Rise. *Nature*, *451*(7175), 181–184. https://doi.org/10.1038/nature06424

Tontoni, F. C., Crone, T. J., deRonde, C. E. J., Fornari, D. J., Kinsey, J. C., Mittelstaedt, E., & Tivey, M. (2016). Crustal magnetization and the subseafloor structure of the ASHES vent field, Axial Seamount, Juan de Fuca Ridge: Implications for the investigation of hydrothermal sites. *Geophysical Research Letters*, *43*. https://doi.org/10.1002/2016GL069430

Travis, B. J., Paguta, J., & Schubert, G. (2012). A whole-moon thermal history model of Europa: Impact of hydrothermal circulation and salt transport. *Icarus*, *218*(2), 1006–1019. https://doi.org/10.1016/j.icarus.2012.02.008

Vance, S., Harnmeijer, J., Kimura, J., Hussmann, H., DeMartin, B., & Brown, J. M. (2007). Hydrothermal systems in small ocean planets. *Astrobiology*, *7*(6), 987–1005. https://doi.org/10.1089/ast.2007.0075

Veirs, S. R., McDuff, R. E., & Stahr, F. R. (2006). Magnitude and variance of near-bottom horizontal heat flux at the Main Endeavour hydrothermal vent field. *Geochemistry, Geophysics, Geosystems*, *7*(2). https://doi.org/10.1029/2005GC000952

Villinger, H., Grevemeyer, I., Hauschild, N. K. J., & Pfender, M. (2002). Hydrothermal heat flux through aged oceanic crust: Where does the heat escape? *Earth and Planetary Science Letters*, *202*. https://doi.org/10.1016/S0012-821X(02)00759-8

Wheat, C. G., Hulme, S. M., Fisher, A. T., Orcutt, B. N., & Becker, K. (2013). Seawater recharge into oceanic crust: IODP Exp 327 Site U1363 Grizzly Bare outcrop. *Geochemistry, Geophysics, Geosystems*, *14*(6), 1957–1972. https://doi.org/10.1002/ggge.20131

Wheat, C. G., & Mottl, M. J. (2000). Composition of pore and spring waters from Baby Bare: Global implications of geochemical fluxes from a ridge flank hydrothermal system. *Geochimica et Cosmochimica Acta*, *64*(4), 629–642. https://doi.org/10.1016/S0016-7037(99)00347-6

Wheat, C. G., Mottl, M. J., Fisher, A. T., & Hulme, S. (2022). Formation waters delineate diverse hydrogeologic conditions at a plate scale: Eastern flank of the Juan de Fuca Ridge. *Geochemistry, Geophysics, Geosystems*, *23*(11), e2022GC010665. https://doi.org/10.1029/2022GC010665

Wheat, C. G., Mottl, M. J., Fisher, A. T., Kadko, D., Davis, E. E., & Baker, E. (2004). Heat and fluid flow through a basaltic outcrop on a ridge flank. *Geochemistry, Geophysics, Geosystems*, *5*(12). https://doi.org/10.1029/2004GC000700

Winslow, D. M., & Fisher, A. T. (2015). Sustainability and dynamics of outcrop-to-outcrop hydrothermal circulation. *Nature Communications*, *6*(1), 7567. https://doi.org/10.1038/ncomms8567

Winslow, D. M., Fisher, A. T., Stauffer, P. H., Gable, C. W., & Zyvoloski, G. A. (2016). Three-dimensional modeling of outcrop-to-outcrop hydrothermal circulation on the eastern flank of the Juan de Fuca Ridge. *Journal of Geophysical Research*, *121*(3), 1365–1382. https://doi.org/10.1002/2015JB012606

Wolery, T. J. (2010). EQ3/6 A software package for geochemical modeling, version 8. https://doi.org/10.11578/dc.20210416.44

Zandenel, A., Truche, L., Hellmann, R., Myagkiy, A., Choblet, G., & Tobie, G. (2021). Short lifespans of serpentinization in the rocky core of Enceladus: Implications for hydrogen production. *Icarus*, *364*. https://doi.org/10.1016/j.icarus.2021.114461

15252027, 2026, 10, Downloaded from https://agupubs.onlinelibrary.wiley.com/doi/10.1029/2026GC012972, Wiley Online Library on [28/10/2026]. See the Terms and Conditions (https://onlinelibrary.wiley.com/terms-and-conditions) on Wiley Online Library for rules of use; OA articles are governed by the applicable Creative Commons License